SIMULATION OF SURFACE WAVES GENERATED BY A RAPID RISE OF A BLOCK AT THE SEA BOTTOM

A THESIS SUBMITTED TO
THE GRADUATE SCHOOL OF NATURAL AND APPLIED SCIENCES
OF
MIDDLE EAST TECHNICAL UNIVERSITY

BY

NALAN ŞENOL

IN PARTIAL FULFILLMENT OF THE REQUIREMENTS
FOR
THE DEGREE OF MASTER OF SCIENCE
IN
CIVIL ENGINEERING

JULY 2005

Approval of the Graduate School of Natural and Applied Sciences

—————————————————

Prof. Dr. Canan ÖZGEN

Director

I certify that this thesis satisfies all the requirements as a thesis for the degree of Master of Science.

—————————————————

Prof. Dr. Erdal ÇOKÇA

Head of Department

This is to certify that we have read this thesis and that in our opinion it is fully adequate, in scope and quality, as a thesis for the degree of Master of Science.

—————————————————

Assoc. Prof. Dr. İsmail AYDIN

Supervisor

Examining Committee Members:

Prof. Dr. Cahit ÇIRAY   (METU,AE) ————————————

Assoc. Prof. Dr. İsmail AYDIN   (METU,CE) ————————————
nnnnnnn

Prof. Dr. Mustafa GÖĞÜŞ   (METU,CE) ————————————

Assoc. Prof. Dr. Zafer BOZKUŞ   (METU,CE) ————————————

Asst. Prof. Dr. Burcu ALTAN SAKARYA (METU,CE) ————————————

I hereby declare that all information in this document has been obtained and presented in accordance with academic rules and ethical conduct. I also declare that, as required by these rules and conduct, I have fully cited and referenced all material and results that are not original to this work.

Name, Last name : Nalan ŞENOL

Signature   :

ABSTRACT

SIMULATION OF SURFACE WAVES GENERATED BY A RAPID RISE OF A BLOCK AT THE SEA BOTTOM

ŞENOL, Nalan
M.Sc., Department of Civil Engineering,
Supervisor: Assoc. Prof. Dr. İsmail AYDIN

July 2005, 74 Pages

A mathematical model is developed for investigating time dependent surface deformations of a hydrostatic water volume, when it is subjected to a sudden partial rise of the sea bottom.

In the model, 2-dimensional, compressible, and viscous Navier-Stokes equations are solved by Marker and Cell (MAC) method. Variable mesh size in both horizontal and vertical directions with a staggered grid arrangement is used. Limited compressibility model is utilized for pressure. Various computational tests are done for the selection of computational parameters of the model. It is found that the amplitude of surface waves generated by vertical displacements of the sea bottom depends on size and speed of bottom displacements.

Keywords: Tsunami generation, moving solid boundary, earthquake, Navier-Stokes Equations, limited compressibility.

ÖZ

DENİZ TABANINDAN BİR BLOĞUN ANİ YÜKSELMESİ SONUCU OLUŞAN YÜZEY DALGALARININ SİMÜLASYONU

ŞENOL, Nalan
Yüksek Lisans, İnşaat Mühendisliği Bölümü,
Danışman: Doç. Dr. İsmail AYDIN

Temmuz 2005, 74 Sayfa

Deniz tabanında gerçekleşen ani kısmi yükselmeye maruz kalan hidrostatik su hacminin zamana bağlı serbest yüzey deformasyonlarını incelemek amacıyla bir matematiksel model oluşturulmuştur.

Modelde viskoz ve sıkıştırılabilir sıvı için Marker and Cell (MAC) Metodu kullanılarak iki-boyutlu Navier-Stokes Denklemlerinin çözümü yapılmıştır. Yatay ve düşey eksende değişken bir ızgara sistemi düzenlenmiştir. Basınç denklemi için sınırlı sıkışabilirlik modelinden yararlanılmıştır. Model parametrelerinin seçimi için çeşitli testler uygulanmıştır. Deniz tabanındaki düşey yönde yer değişimlerin oluşturduğu yüzey dalgalarının genliğinin, yer değiştiren tabanın büyüklüğüne ve hızına bağlı olduğu bulunmuştur.

Anahtar kelimeler: Tsunami oluşumu, hareketli katı sınır, deprem, Navier-Stokes denklemleri, sınırlı sıkışabilirlik.

Dedicated to My Family

ACKNOWLEDGEMENTS

TABLE OF CONTENTS

LIST OF TABLES

TABLE

LIST OF FIGURES

FIGURE

LIST OF SYMBOLS

c : Speed of sound

δt : Time increment for the forward time discretization

δx_i : Width of computational cell, variable

$\delta x e_i$: Horizontal distance between the cell centers of the east neighbor cell and the cell in the ith column

$\delta x w_i$: Horizontal distance between the cell centers of the west neighbor cell and the cell in the ith column

δz_j : Height of computational cell, variable

$\delta z n_j$: Vertical distance between the cell centers of the north neighbor cell and the cell in j^{th} row

$\delta z s_j$: Vertical distance between the cell centers of the south neighbor cell and the cell in j^{th} row

g_x : Body acceleration in x-direction

g_z : Body acceleration in z-direction

γ : Weighting parameter for central differences and donor cell discretization

θ : Weighting parameter for dissipation term of surface height equation

h : Surface height of fluid

h_i : Surface height at i^{th} discrete column of fluid

h_{max} : Maximum recorded surface height of entire fluid at an instant of time

h_0 : Surface height of fluid at the column on the symmetry line

H : Initial water depth

H_S : Block height

i : Space index in horizontal direction for discrete parameters

j : Space index in vertical direction for discrete parameters

L_R : Computational domain length

L_S : Moving block length

μ : Absolute viscosity of fluid

n : Time step index for discrete parameters

v : Kinematic viscosity of fluid

ω : Relaxation parameter for SOR method

P : Pressure

p : Pressure normalized by fluid density

$P_{surface}$: Pressure on the free surface

ρ : Density

σ_{xx} : Normal component of momentum per unit density flowing per unit time in x direction through unit area in x direction

σ_{zz} : Normal component of momentum per unit density flowing per unit time in z direction through unit area in z direction

t : Time

τ_{xz} : Tangential component of momentum per unit density flowing per unit time in z direction through unit area in x direction

τ_{zx} : Tangential component of momentum per unit density flowing per unit time in x direction through unit area in z direction

u : Velocity component in x-direction

w : Velocity component in z-direction

$u_{surface}$: Velocity component in x-direction on the free surface

$w_{surface}$: Velocity component in z-direction on the free surface

W_{block} : Block velocity

W_{max} : Maximum block velocity

x : Spatial variable in horizontal direction

z : Spatial variable in vertical direction

CHAPTER I

INTRODUCTION

1.1 Earthquakes and Tsunamis in the World

1.1.1 Tsunami: Generation and Propagation

Tsunami is a natural phenomenon, which ranks high on the scale of natural disasters, consisting of a series of waves generated when water in a lake or the sea is rapidly displaced on a massive scale.

Earthquakes, landslides, volcanic eruptions and large meteorite impacts all have the potential to generate a tsunami. The effects of a tsunami can range from unnoticeable to devastating [1].

A tsunami is not a sub-surface event in the deep ocean; it simply has much smaller amplitude offshore, and often hundreds of kilometers long wavelength, which is why they generally pass unnoticed at sea, forming only a passing "hump" in the ocean [1].

1.1.1.1 Generation

Tsunami can be generated by any disturbance that rapidly displaces a large mass of water, such as an earthquake, volcanic eruption, landslide or meteorite impact. However, the most common cause is an undersea earthquake. An earthquake which

is too small to create a tsunami by itself may trigger an undersea landslide quite capable of generating a tsunami.

Tsunamis can be generated when the sea floor abruptly deforms and vertically displaces the overlying water. Such large vertical movements of the earth's crust can occur at plate boundaries [2].

Submarine landslides; which are sometimes triggered by large earthquakes; as well as collapses of volcanic edifices, may also disturb the overlying water column as sediment and rocks slide downslope and are redistributed across the sea floor. Similarly, a violent submarine volcanic eruption can uplift the water column and generate a tsunami [1].

Tsunami is a set of ocean waves caused by any large, abrupt disturbance of the sea-surface. If the disturbance is close to the coastline, local tsunamis can demolish coastal communities within minutes. A very large disturbance can cause local devastation and export tsunami destruction thousands of kilometers away.

They frequently occur in the Pacific, where dense oceanic plates slide under the lighter continental plates. When these plates fracture they provide a vertical movement of the seafloor that allows a quick and efficient transfer of energy from the solid earth to the ocean [1].

Other large-scale disturbances of the sea -surface that can generate tsunamis are explosive volcanoes and asteroid impacts.

"Tsunamis occur most frequently in the Pacific Ocean, but are a global phenomenon; they are possible wherever large bodies of water are found - including inland lakes" [1].

1.1.1.2 Propagation

"Predicting when and where the next tsunami will strike is currently impossible, but once generated, forecasting tsunami arrival and impact is possible through existing wave theory and new measurement technology"[2].

Most of the damage is caused by the huge mass of water behind the initial wave front, as the height of the sea keeps rising fast and floods powerfully into the coastal area.

Tsunamis act very differently from typical surf swells. They move the entire depth of the ocean (often several kilometers deep) rather than just the surface, so they contain immense energy, propagate at high speeds and can travel great transoceanic distances with little overall energy loss. A tsunami can cause damage at places thousands of kilometers from its origin, so there may be several hours between its creation and its impact on a coast, arriving long after the seismic wave generated by the originating event arrives [2].

In open water, tsunamis have extremely long periods, from minutes to hours, and long wavelengths of up to several hundred kilometers. The actual height of a tsunami wave in open water is often less than one meter. This is often practically unnoticeable to people on ships [2].

The wave travels across the ocean at speeds from 500 to 1,000 km/h. As the wave approaches land, the sea shallows and the wave no longer travel as quickly, so it begins to 'pile-up'; the wave-front becomes steeper and taller, and there is less distance between crests [2].

A wave becomes a 'shallow-water wave' when the ratio between the water depth and its wavelength gets very small, and since a tsunami has an extremely large wavelength (hundreds of kilometers), tsunamis act as a shallow-water wave even in deep oceanic water [2].

Earth movements associated with large earthquakes are thousand of square kilometers in area. Therefore, any vertical movement of the seafloor, immediately changes the sea-surface.

1.1.2 2004-Indian Ocean Tsunami

When a powerful earthquake struck the coastal region of Indonesia in 2004, the movement of the seafloor produced a tsunami in excess of 30 meters along the adjacent coastline [3].

2004 Indian Ocean Earthquake triggered a series of lethal tsunamis on December 26, 2004 that killed over 310,000 people, making it the deadliest tsunami in recorded history. The tsunami killed people over an area ranging from the immediate vicinity of the quake in Indonesia, Thailand and the north-western coast of Malaysia to thousands of kilometers away in Bangladesh, India, Sri Lanka, the Maldives, and even as far as Somalia, Kenya and Tanzania in eastern Africa [3].

The 2004 Indian Ocean earthquake was an undersea earthquake at the magnitude of 9.0. It is a megathrust earthquake, which is an interplate earthquake where one tectonic plate slips beneath another. This kind of earthquake mostly occurs in the Pacific and Indian Oceans. Since these earthquakes deform the ocean floor, they almost always generate a significant tsunami [3].

People still do not know which waves cause a tsunami. After the earthquake in Sumatra a great tsunami is seen but in three months time another earthquake happened, with approximately same in scale as the previous one, and did not form a tsunami, indeed most researchers were waiting for one.

The earthquake on December 26, 2004 was unusually large in geographical extent. An estimated 1200 km of fault line slipped about 15 m along the subduction zone where the India Plate dives under the Burma Plate. The slip did not happen instantaneously but took place in two phases over a period of several minutes. Seismographic data indicate that the first phase involved the formation of a rupture about 400 km long and 100 km wide, located 30 km beneath the sea bed. The rupture proceeded at a speed of about 2 km/s or 7200 km/h, beginning off the coast of Aceh and proceeding north-westerly over a period of about 100 seconds. A pause of about another 100 seconds took place before the rupture continued northwards towards the Andaman and Nicobar Islands [3].

As well as the sideways movement between the plates, the sea bed is estimated to have risen by several meters, triggering devastating tsunami waves.

"The sudden vertical rise of the seabed by several meters during the earthquake displaced massive volumes of water, resulting in a tsunami that struck the coasts of the Indian Ocean" [3].

1.2 Earthquakes and Tsunamis in Turkey

Numerous large destructive earthquakes and tsunamis have occurred from antiquity to the present in the Ionian Sea, Greece, the Aegean Archipelago, Turkey and the Sea of Marmara - which separates Asia Minor from Europe. Most of the destructive tsunamis in the past originated from a region of the Hellenic arc where normal

5

faulting within the southern part of the Anatolian Tectonic Plate (the Aegean plate) is consistent with a NE-SW trending graben along which the Santorin volcanic field has also developed [4].
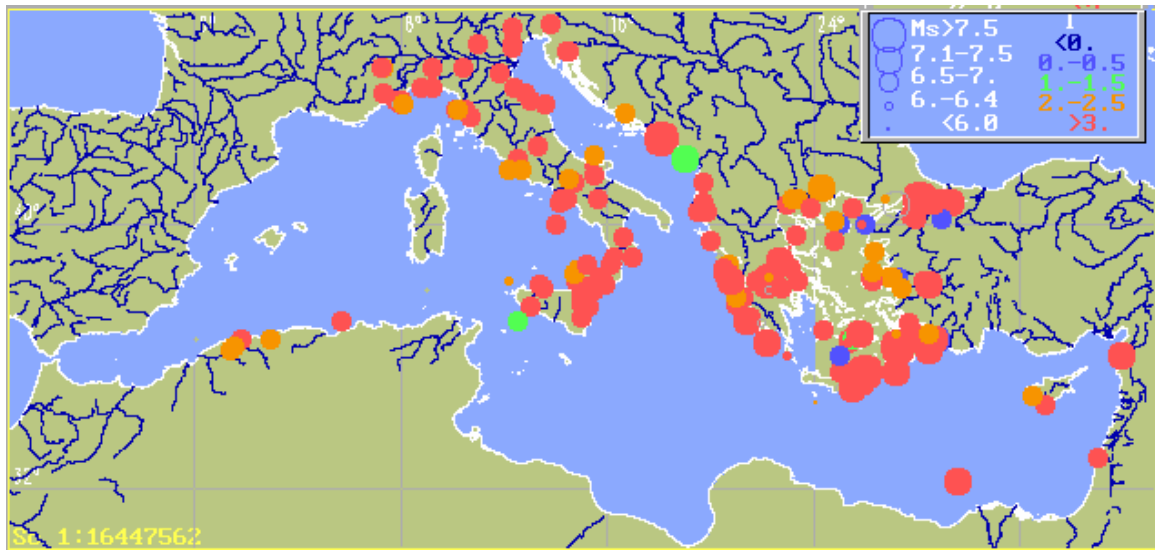
Figure 1.1 Historical tsunami events in the Mediterranean region [5]

In Fig.1.1 the size of circle is proportional to the event magnitude. The preliminary version of the regional tsunami catalog [5] covers the period from 1500 to 1990 and contains 297 events. However, not all events are presented on this map, because 91 events lack their source coordinates.

Although most of the earthquakes along the great North Anatolian fault involve primarily horizontal ground displacements - and such tectonic movements do not ordinarily generate tsunamis - some of the earthquakes along the western segment of the fault have triggered major slumps that have generated tsunamis. At least 9 major tsunamis have been reported to have occurred in the Marmara Sea in the past [6].

1.2.1 August 17, 1999 Sea of Marmara Earthquake

On August 17, 1999, a large destructive earthquake struck northwest Turkey and generated a local tsunami within the enclosed Sea of Marmara. This was the strongest earthquake to strike Northern Turkey since 1967. It occurred along the Northern Anatolian fault. Its epicenter was in the Gulf of Izmit [7].

The earthquake of August 17, 1999 occurred along the long, east-west trending, great North Anatolian Fault Zone (NAFZ) - known to be the most prominent active fault system in Northwestern Turkey. NAFZ passes through Izmit Bay, traverses Marmara Sea and reaches the Saros Gulf to the southeast. This great fault system has many similarities to the San Andreas Fault system in California. Earthquakes involve primarily horizontal ground motions (strike-slip type of faulting) [4].

Ground displacements between Lake Sapanca and the Gulf of Izmit were about 2.60 m. Additionally, there was evidence of about 2 meters subsidence along the north side of the fault's block - which was particularly evident along the coastline at Golcuk, where tsunami waves and major flooding occurred. Such tectonic ground displacements are characteristic of major earthquakes along the North Anatolian Fault and, possibly, have been responsible for tsunami generation in the past [4].

It appears that most of the seismic strain along this section of the North Anatolian fault was released by the August 17, 1999 earthquake. However, given the measurements of 1.5 meter ground displacements in the Akyazi area, versus the larger displacements elsewhere, it is quite possible that not all of the seismic strain was released by this event and that some future seismic event will release the remaining strain [4].

Although the earthquake involved primarily horizontal ground displacements, slumping and landslides triggered tsunami waves which were particularly damaging in the Gulf of Izmit, perhaps because of convergence and a funneling effect. The long duration of the earthquake's ground motions (45 seconds), the directivity of the surface seismic waves, the proximity of the epicenter to the Sea of Marmara and the Gulf of Izmit, and the overall orientation of the affected area, strongly support that the tsunami was generated in the Gulf of Izmit, in the eastern portion of the Sea of Marmara [4].

An initial recession of the water was observed at both sides of Izmit Bay immediately after the quake, followed by tsunami waves which had an average run-up of 2.5 m. along the coast. Maximum run-up was 4 m in Golcuk where there was considerable damage to the naval base facilities. In fact, Golcuk and several coastal areas are then flooded permanently as a result of the tectonic subsidence and landslides [8].

After this devastating disaster, according to Barka et al. [8], it is obvious that the tsunami risk for the Sea of Marmara needs to be carefully evaluated.

1.3 Problem Definition

The aim of this study is to determine surface wave histories due to the bottom block movement. Starting from a steady fluid domain, a finite block at the bottom is assumed to move suddenly in vertical direction and consequences of sudden movement of the bottom on the pressure distribution and subsequent surface deformations are investigated.
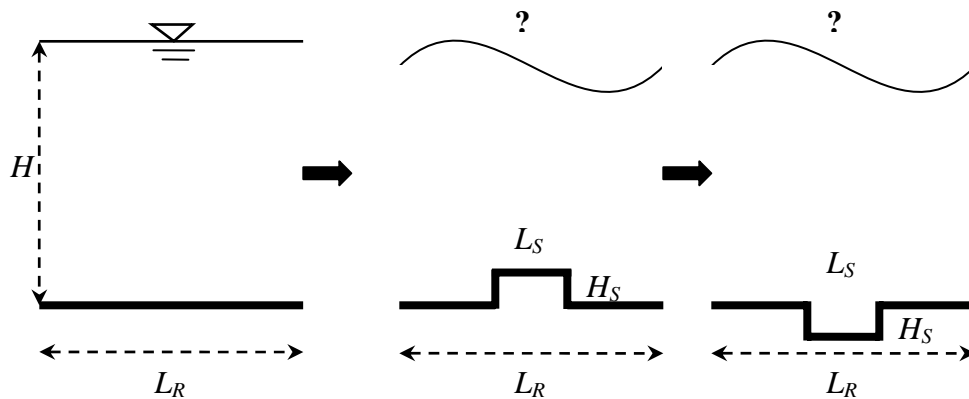
Figure 1.2 Description of the problem

The forcing mechanism can be in two directions, upward or downward movement of the bottom. Since the downward movement is just the analogous to the former one from computational point of view, in this study only upward excitation is solved.

In nature, generally fault cracks are not as uniform as the one considered in this model, but the physical effect to the domain of the natural case and the one used here are similar. Therefore, for the sake of simplicity, a rectangular bottom portion movement in upward direction is used as the excitation. As can be seen from Fig.1.2, H is the initial water height, L_R is the width of the domain affected from the movement, L_S is the width of the moving portion, and H_S is the height of the differential rise or drop.

1.4 Literature Review

Lynett and Liu [9], for instance, derived a mathematical model to describe the generation and propagation of water waves by a submarine landslide. The model consists of a depth-integrated continuity equation and a momentum equation, in

which the ground movement is a forcing function. They also study on propagation from relatively deep water to shallow water for the sake of completeness. As a case study, tsunamis generated by a prehistoric massive submarine slump off the northern coast of Puerto Rico are modeled.

Similar to the study of Lynett and Liu [9], Todorovska et al. [10] are also searching on the near-field amplitudes of Tsunami from submarine slumps and slides, which are the common causes of tsunami generations. According to them, the common mechanisms for triggering failure of submarine slopes are over-steepening due to rapid deposition of sediments, generation of gas created by decomposition of organic matter, storm waves, and earthquakes, which are the major cause of landslides on continental slopes. To reflect the real situation they have used five 2D, kinematic source models that consider the effects of source finiteness and directivity.

As can be seen from Fig. 1.3, Model 1A represents sliding down hill, while Model 1B represents spreading of the source area up hill and down hill, at different rates. Model 2 is a schematic representation of a rotational slide and Model 3 represents the landslide [10].

Fine et al. [11] are dealing with the recent catastrophic tsunamis at Flores Island, Indonesia (1992), Skagway, Alaska (1994), Papua New Guinea (1998), and İzmit, Turkey (1999). They have noticed that purely submarine slides are ineffective at tsunami generation compared with subaerial slides. In addition, they have found that a rigid-body slide produces much higher tsunami waves than a viscous slide.

10
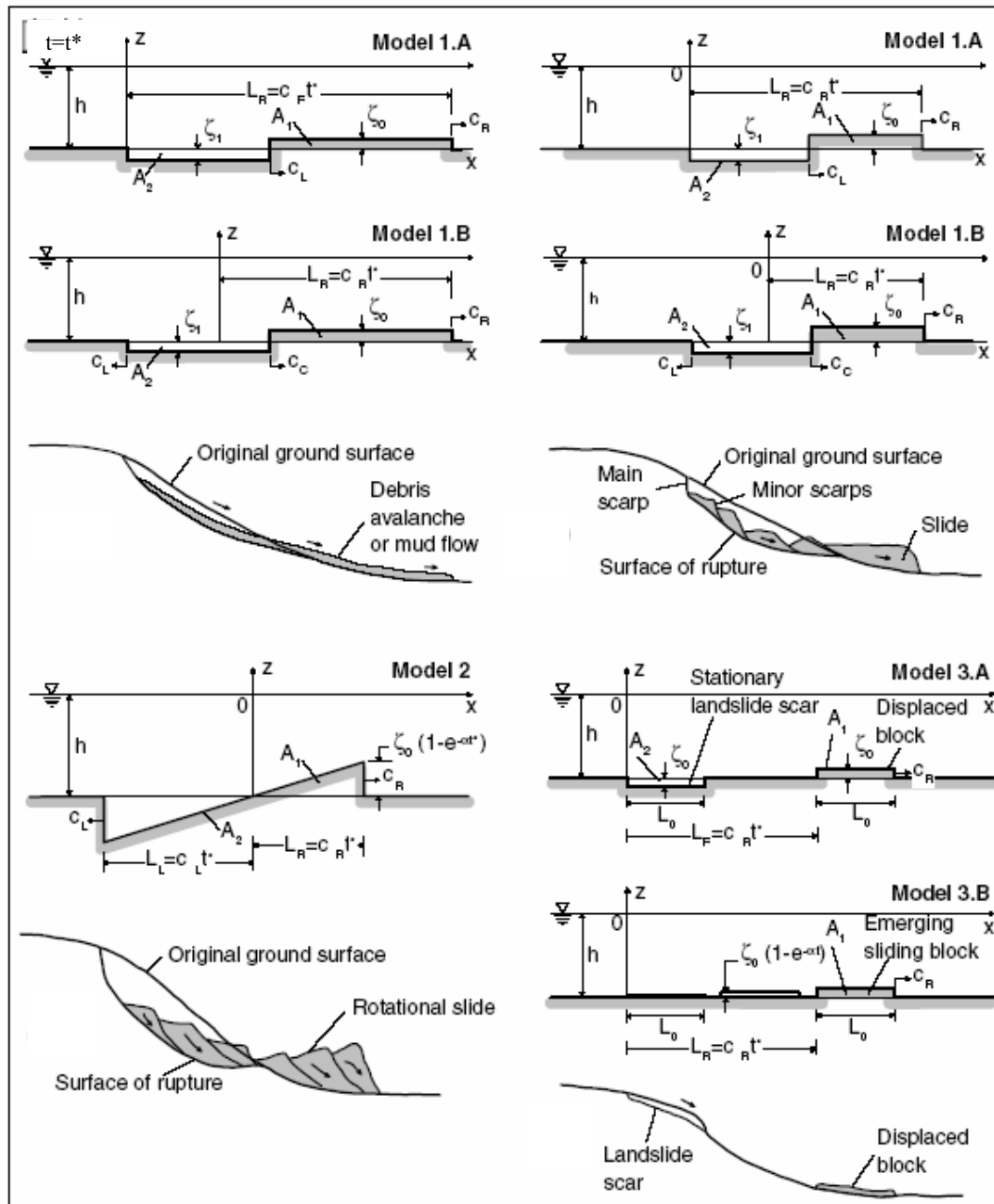
Figure 1.3 Tsunami generation mechanisms [10]

In parallel with this thesis, Ohmachi [12] uses velocity associated with the seabed displacement as the input accordingly at the bottom of the seawater. Then the resulting seawater disturbance is simulated by solving the Navier-Stokes equations

without using the long wave approximation, and introducing a height function. The CFL condition is utilized for stability purposes. The 2D tsunami simulation model of Ohmachi [12] is seen in Fig.1.4;
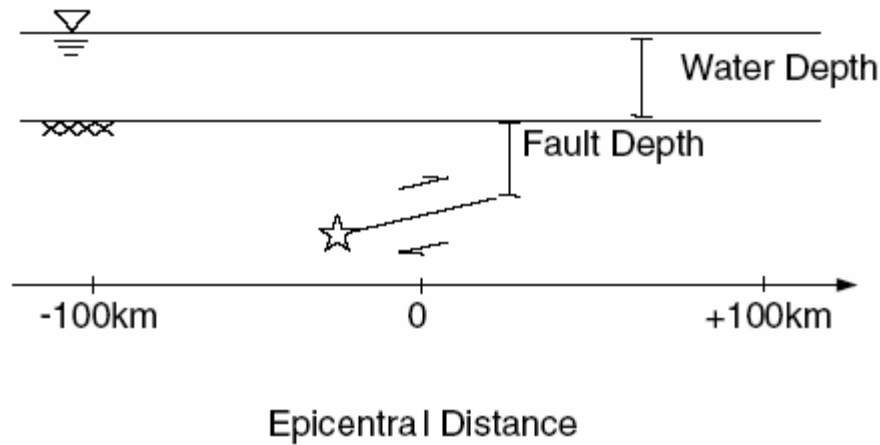
Figure 1.4 2D-Tsunami simulation model [12]

Tyvand et al. [13] are considering the effect of a rising block by integrating the Fourier and Green functions numerically. In their paper tsunami generation due to impulsive bottom deflections which are reported as "rapid".

According to Tyvand, Miloh and Haugen [13], bottom movement that endures shorter than the gravitational time, i.e $(h/g)^{1/2}$, where h is the initial ocean depth and g is the gravitational acceleration, is named as sudden. They propose that this constraint may apply to tsunamis generated by earthquakes, but not to tsunamis due to landslides or volcanic eruptions. They claim that the traditional tsunami generation models due to rapid bottom motion often take the surface deflection to be the same as that of the bottom.

In their study on the effects of tsunami at Sissano Lagoons, Papua New Guinea, Matsuyama and Yeh [14] stated that the primary cause of the discrepancy in

tsunami run-up height and pattern between the observation and the initial numerical prediction is the use of faulty bathymetry data.

In his study Kırlangıç [15], solves two-dimensional Navier-Stokes Equations on a vertical plane numerically by using Marker and Cell Method for viscous and compressible fluid including all the nonlinear effects in the solution. Grid clustering in vertical direction is utilized. The excitation of the system, sudden block movement, is modeled as zigzag motion. Limited compressibility method is used for pressure equation. The program NaSt2D, constructed by Griebel et al. [16] is used with modifications according to the problem of the study.

1.4.1 Density Variation with respect to Depth

The role of water compressibility in the tsunami problem has been discussed many times. It is well known that submarine earthquakes can radiate not only gravitational but also hydroacoustic waves. However, in most cases, tsunami is considered as a process in incompressible fluid [17].

Two Russian researchers Nosov and Kolesov [17] present their studies on tsunami wave generation by small bottom displacements in compressible ocean of variable depth. Linear potential theory is considered. According to them, if the computational domain is large and the bottom displacement takes place in a short duration, fluid should be considered as compressible.

In order to verify the analytical method, the change in the density of the sea water [18] is calculated according to the UNESCO International Equation of State (IES 80) standards [19]. Water density depends mainly on pressure, temperature and

salinity. Here temperature is taken to be 10°C and salinity to be 20[1]. These values are comparable to real values of the seas around Turkey [20]. Hydrostatic calculations show that the variation in the density is no more than 3 parts in 1000. Hence it is viable to assume that the density is constant in the analytical derivation wherever necessary. Though, the corrected densities are calculated for the initial case and every time step for each cell.

1.5 Scope of the Study

Up to recent studies, researchers mostly studied on simulations of tsunami propagation. Because of the uncertainty where and when a crack will happen on the bottom of an ocean for instance, there is not any field data available. Therefore, the physical behavior of those disasters is usually predicted by numerical solutions. Different mathematical models are used. In those models Navier-Stokes equations are preferred by considering finite volume, finite difference, finite element, and volume of fluid methods.

The aim of this thesis is to develop a computer program that solves 2D, compressible Navier-Stokes equations in a vertical plane for a viscous fluid, to investigate the effect of sudden partial bottom movement to the pressure field and the resulting free surface waves in the computational domain.

FORTRAN is preferred as the programming language. Variable mesh is used in both vertical and horizontal directions to increase the resolution in the critical

---

[1] Practical salinity of a sample of seawater, is defined in terms of the ratio K_{15} of the electrical conductivity of the seawater sample at the temperature of 15°C and the pressure of one standard atmosphere, to that of a potassium chloride (KCl) solution, in which the mass fraction of KCl is 32.4356E-3, at the same temperature and pressure.

sections. Limited compressibility formulation [21] is used in pressure solution. Surface Height Method [22] is utilized for the free surface treatment.

CHAPTER II

MATHEMATICAL MODEL

2.1 Governing Equations

The differential equations that form the mathematical model of this study are the continuity equation (2.1), the momentum equations (2.2, 2.3) and the free surface equation that describes the change in water depth (2.4).

$$\frac{\partial \rho}{\partial t} + u\frac{\partial \rho}{\partial x} + w\frac{\partial \rho}{\partial z} + \rho\left(\frac{\partial u}{\partial x} + \frac{\partial w}{\partial z}\right) = 0 \tag{2.1}$$

$$\rho\left(\frac{\partial u}{\partial t} + u\frac{\partial u}{\partial x} + w\frac{\partial u}{\partial z}\right) = \rho g_x - \frac{\partial P}{\partial x} + \mu\left(\frac{\partial^2 u}{\partial x^2} + \frac{\partial^2 u}{\partial z^2}\right) + \frac{\mu}{3}\frac{\partial}{\partial x}\left(\frac{\partial u}{\partial x} + \frac{\partial w}{\partial z}\right) \tag{2.2}$$

$$\rho\left(\frac{\partial w}{\partial t} + u\frac{\partial w}{\partial x} + w\frac{\partial w}{\partial z}\right) = \rho g_z - \frac{\partial P}{\partial z} + \mu\left(\frac{\partial^2 w}{\partial x^2} + \frac{\partial^2 w}{\partial z^2}\right) + \frac{\mu}{3}\frac{\partial}{\partial z}\left(\frac{\partial u}{\partial x} + \frac{\partial w}{\partial z}\right) \tag{2.3}$$

$$\frac{\partial h}{\partial t} = w_{surface} - u_{surface}\frac{\partial h}{\partial x} \tag{2.4}$$

In the above equations x and z are spatial variables in horizontal and vertical directions, respectively, t is time, ρ is the density of the fluid, u and w are the velocity components in horizontal and vertical directions respectively, P is the pressure, μ is the dynamic viscosity, and g_x and g_z are the body accelerations in horizontal and vertical directions, respectively.

2.2 Generation of the Model

The mathematical model of this study is generated from the program NaSt2D, constructed by Griebel et al. [16] by using FORTRAN. NaSt2D is a general code that solves two-dimensional Navier-Stokes Equations for incompressible viscous fluids by using constant mesh.

The model of Griebel et al. [16] is modified to reflect the problem of this study by incorporating computational mesh variation in both horizontal and vertical directions, clustering in grid generation, partial sudden bottom movement and Limited Compressibility Method for pressure solution.

2.3 Limited Compressibility Method

According to the study of Hirt and Nichols [21], pressure is assumed to be only a function of fluid density.
The following equation shows the relation between the fluid pressure and density in terms of adiabatic speed of sound, c.

$$\frac{dP}{d\rho} = c^2 \tag{2.5}$$

c may be time- or space- or temperature-dependent parameter, for the sake of simplicity it is assumed to be constant as 1482 m/s.

The mass conservation equation (2.1) can be rewritten by using equation (2.5);

$$\frac{1}{c^2}\frac{\partial P}{\partial t} + \frac{1}{c^2}\left(u\frac{\partial P}{\partial x} + w\frac{\partial P}{\partial z}\right) + \rho\left(\frac{\partial u}{\partial x} + \frac{\partial w}{\partial z}\right) = 0 \tag{2.6}$$

Since the values of u/c^2 and w/c^2 will be very small, the above equation can be further simplified by neglecting spatial variations of density,

$$\frac{\partial P}{\partial t} = -c^2 \rho \left(\frac{\partial u}{\partial x} + \frac{\partial w}{\partial z} \right) \tag{2.7}$$

Before discretization, the governing equations are divided by fluid density and rewritten,

$$\frac{\partial p}{\partial t} = -c^2 \left(\frac{\partial u}{\partial x} + \frac{\partial w}{\partial z} \right) \tag{2.8}$$

$$\frac{\partial u}{\partial t} + u \frac{\partial u}{\partial x} + w \frac{\partial u}{\partial z} = -\frac{\partial p}{\partial x} + g_x + \frac{\mu}{\rho} \left(\frac{\partial^2 u}{\partial x^2} + \frac{\partial^2 u}{\partial z^2} \right) + \frac{\mu}{3\rho} \frac{\partial}{\partial x} \left(\frac{\partial u}{\partial x} + \frac{\partial w}{\partial z} \right) \tag{2.9}$$

$$\frac{\partial w}{\partial t} + u \frac{\partial w}{\partial x} + w \frac{\partial w}{\partial z} = -\frac{\partial p}{\partial z} + g_z + \frac{\mu}{\rho} \left(\frac{\partial^2 w}{\partial x^2} + \frac{\partial^2 w}{\partial z^2} \right) + \frac{\mu}{3\rho} \frac{\partial}{\partial z} \left(\frac{\partial u}{\partial x} + \frac{\partial w}{\partial z} \right) \tag{2.10}$$

where p is the pressure normalized by density, that is:

$$p = \frac{P}{\rho} \tag{2.11}$$

2.4 Discretization

The computational mesh is variable in both x- and z-directions. Staggered grid system is used in which the velocity components are defined at the cell faces while the pressure is defined at the cell center. Notation used is given in Fig 2.1. For the cell$_{i,j}$, δx_i is the horizontal distance, $\delta x w_i$ is the horizontal distance between the west neighbor cell center and the center of the cell$_{i,j}$. Similarly, $\delta x e_i$ is the horizontal distance between the east neighbor cell center and the center of the cell$_{i,j}$. Vertical distance of the corresponding cell is named as δz_j. $\delta z n_j$ and $\delta z s_j$ are the distances between the neighboring cell centers.

18
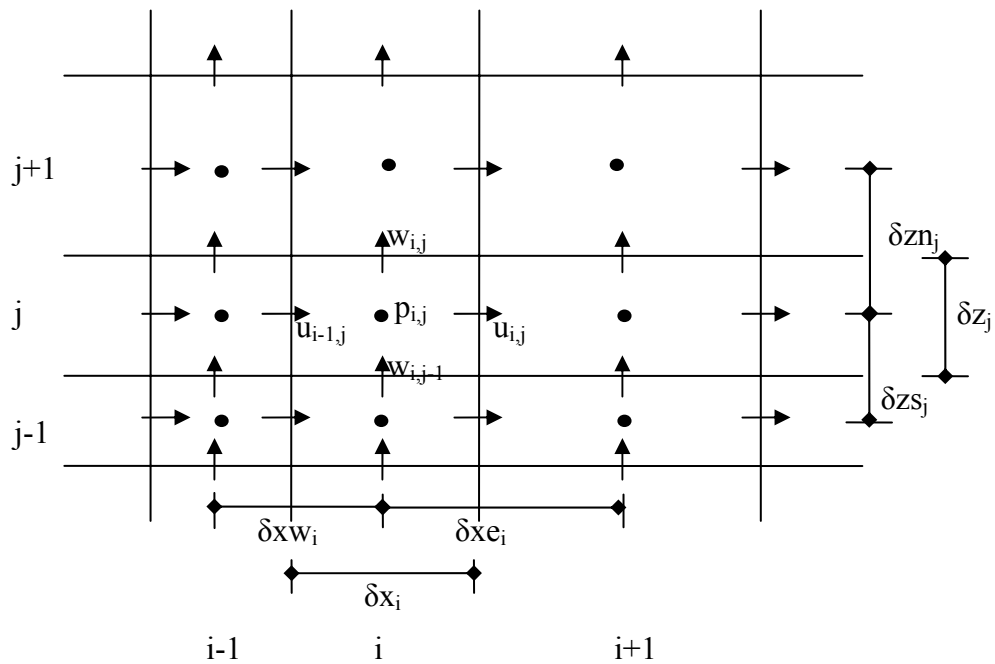
Figure 2.1 Staggered grid system

The convective terms in the momentum equations are discretized by considering a combination of central differences and donor cell discretizations;

Convective Terms = (1-γ)[Central Differences] + γ[Donor Cell Differencing] **(2.12)**

The reason is the dominancy of the convective terms of the momentum equations at high velocities. If only the convective terms are dominant, diffusive terms are recessive so stability problems may occur. To avoid those problems, γ, a parameter that gives control to the discretization method, is utilized. As can be seen from the above combination of central difference and donor cell discretization methods, γ should take a value between 0 and 1. For $\gamma = 1$ central difference terms are omitted so the whole system discretized by donor cell scheme [16].

Horizontal and vertical distances from the neighboring cell centers to the center of the cell(i,j) can be defined as;

$$\delta xw_i = \frac{\delta x_i + \delta x_{i-1}}{2} \qquad (2.13)$$

$$\delta xe_i = \frac{\delta x_i + \delta x_{i+1}}{2} \qquad (2.14)$$

$$\delta zs_j = \frac{\delta z_j + \delta z_{j-1}}{2} \qquad (2.15)$$

$$\delta zn_j = \frac{\delta z_j + \delta z_{j+1}}{2} \qquad (2.16)$$

2.4.1 X-Momentum

The momentum equations are discretized as described by Griebel et al. [16]:

$$\left[\frac{\partial u}{\partial x}\right]_{i,j}^{backward} = [DUW]_{i,j} = \frac{u_{i,j} - u_{i-1,j}}{\delta x_i} \qquad (2.17)$$

$$\left[\frac{\partial u}{\partial x}\right]_{i,j}^{forward} = [DUE]_{i,j} = \frac{u_{i+1,j} - u_{i,j}}{\delta x_{i+1}} \qquad (2.18)$$

$$\left[\frac{\partial u}{\partial z}\right]_{i,j}^{backward} = [DUS]_{i,j} = \frac{u_{i,j} - u_{i,j-1}}{\delta zs_j} \qquad (2.19)$$

$$\left[\frac{\partial u}{\partial z}\right]_{i,j}^{forward} = [DUN]_{i,j} = \frac{u_{i,j+1} - u_{i,j}}{\delta zn_j} \qquad (2.20)$$

$$\overline{w}_R = \frac{w_{i+1,j}\delta zs_j + w_{i+1,j-1}\delta zn_j}{\delta zs_j + \delta zn_j} \qquad (2.21)$$

$$\overline{w}_L = \frac{w_{i,j}\,\delta z s_j + w_{i,j-1}\,\delta z n_j}{\delta z s_j + \delta z n_j} \tag{2.22}$$

$$\overline{w}_{i,j} = \frac{\overline{w}_R\,\delta x_i + \overline{w}_L\,\delta x_{i+1}}{\delta x_i + \delta x_{i+1}} \tag{2.23}$$

$$\delta z_\alpha = \delta z n_j + \delta z s_j + \gamma\,\mathrm{sgn}\!\left(\overline{w}_{i,j}\right)\!\left(\delta z n_j - \delta z s_j\right) \tag{2.24}$$

$$\delta x_\alpha = \delta x_{i+1} + \delta x_i + \gamma\,\mathrm{sgn}\!\left(u_{i,j}\right)\!\left(\delta x_{i+1} - \delta x_i\right) \tag{2.25}$$

$$\left[u\frac{\partial u}{\partial x}\right]_{i,j} = [UDUDX]_{i,j} = \frac{u_{i,j}}{\delta x_\alpha}\left(\delta x_{i+1}[DUW]_{i,j} + \delta x_i[DUE]_{i,j}\right)$$
$$+ \frac{u_{i,j}}{\delta x_\alpha}\gamma\,\mathrm{sgn}\!\left(u_{i,j}\right)\!\left(\delta x_{i+1}[DUW]_{i,j} - \delta x_i[DUE]_{i,j}\right) \tag{2.26}$$

$$\left[w\frac{\partial u}{\partial z}\right]_{i,j} = [WDUDZ]_{i,j} = \frac{\overline{w}_{i,j}}{\delta z_\alpha}\left(\delta z n_j[DUS]_{i,j} + \delta z s_j[DUN]_{i,j}\right)$$
$$+ \frac{\overline{w}_{i,j}}{\delta z_\alpha}\gamma\,\mathrm{sgn}\!\left(\overline{w}_{i,j}\right)\!\left(\delta z n_j[DUS]_{i,j} - \delta z s_j[DUN]_{i,j}\right) \tag{2.27}$$

$$\left[\frac{\partial^2 u}{\partial x^2} + \frac{\partial^2 u}{\partial z^2}\right]_{i,j} = [LAPLU]_{i,j}$$
$$\tag{2.28}$$

$$= \frac{2}{\delta x_{i+1} + \delta x_i}\left[\frac{u_{i+1,j} - u_{i,j}}{\delta x_{i+1}} - \frac{u_{i,j} - u_{i-1,j}}{\delta x_i}\right] + \frac{2}{\delta z n_j + \delta z s_j}\left[\frac{u_{i,j+1} - u_{i,j}}{\delta z n_j} - \frac{u_{i,j} - u_{i,j-1}}{\delta z s_j}\right]$$

$$[COMPX]_{i,j} = \frac{2}{\delta x_{i+1} + \delta x_i} \left(\frac{u_{i+1,j} - u_{i,j}}{\delta x_{i+1}} - \frac{u_{i,j} - u_{i-1,j}}{\delta x_i} \right)$$

$$+ \frac{2}{\delta x_{i+1} + \delta x_i} \left(\frac{w_{i+1,j} - w_{i+1,j-1}}{\delta z_j} - \frac{w_{i,j} - w_{i,j-1}}{\delta z_j} \right) \qquad \textbf{(2.29)}$$

$$\left[\frac{\partial p}{\partial x} \right]_{i,j} = \frac{p_{i+1,j} - p_{i,j}}{\delta x e_i} \qquad \textbf{(2.30)}$$

2.4.2 Z-Momentum

For the terms of *z*-momentum equation, similar formulation is utilized as the one used for the *x*-momentum discretization.

$$\left[\frac{\partial w}{\partial x} \right]_{i,j}^{backward} = [DWW]_{i,j} = \frac{w_{i,j} - w_{i-1,j}}{\delta x w_i} \qquad \textbf{(2.31)}$$

$$\left[\frac{\partial w}{\partial x} \right]_{i,j}^{forward} = [DWE]_{i,j} = \frac{w_{i+1,j} - w_{i,j}}{\delta x e_i} \qquad \textbf{(2.32)}$$

$$\left[\frac{\partial w}{\partial z} \right]_{i,j}^{backward} = [DWS]_{i,j} = \frac{w_{i,j} - w_{i,j-1}}{\delta z_j} \qquad \textbf{(2.33)}$$

$$\left[\frac{\partial w}{\partial z} \right]_{i,j}^{forward} = [DWN]_{i,j} = \frac{w_{i,j+1} - w_{i,j}}{\delta z_{j+1}} \qquad \textbf{(2.34)}$$

$$\bar{u}_B = \frac{u_{i-1,j}\delta x e_i + u_{i,j}\delta x w_i}{\delta x e_i + \delta x w_i} \qquad \textbf{(2.35)}$$

$$\bar{u}_T = \frac{u_{i-1,j+1}\delta x e_i + u_{i,j+1}\delta x w_i}{\delta x e_i + \delta x w_i} \qquad \textbf{(2.36)}$$

$$\overline{u}_{i,j} = \frac{\overline{u}_B \delta z_{j+1} + \overline{u}_T \delta z_j}{\delta z_j + \delta z_{j+1}} \tag{2.37}$$

$$\delta z_\alpha = \delta z_{j+1} + \delta z_j + \gamma \operatorname{sgn}(w_{i,j})(\delta z_{j+1} - \delta z_j) \tag{2.38}$$

$$\delta x_\alpha = \delta x e_i + \delta x w_i + \gamma \operatorname{sgn}(\overline{u}_{i,j})(\delta x e_i - \delta x w_i) \tag{2.39}$$

$$\left[u \frac{\partial w}{\partial x} \right]_{i,j} = [UDWDX]_{i,j} = \frac{\overline{u}_{i,j}}{\delta x_\alpha}\left(\delta x e_i [DWW]_{i,j} + \delta x w_i [DWE]_{i,j} \right)$$
$$+ \frac{\overline{u}_{i,j}}{\delta x_\alpha} \gamma \operatorname{sgn}(\overline{u}_{i,j})\left(\delta x e_i [DWW]_{i,j} - \delta x w_i [DWE]_{i,j} \right) \tag{2.40}$$

$$\left[w \frac{\partial w}{\partial z} \right]_{i,j} = [WDWDZ]_{i,j} = \frac{w_{i,j}}{\delta z_\alpha}\left(\delta z_{j+1} [DWS]_{i,j} + \delta z_j [DWN]_{i,j} \right)$$
$$+ \frac{w_{i,j}}{\delta z_\alpha} \gamma \operatorname{sgn}(w_{i,j})\left(\delta z_{j+1} [DWS]_{i,j} - \delta z_j [DWN]_{i,j} \right) \tag{2.41}$$

$$\left[\frac{\partial^2 w}{\partial x^2} + \frac{\partial^2 w}{\partial z^2} \right]_{i,j} = [LAPLW]_{i,j} \tag{2.42}$$

$$= \frac{2}{\delta x e_i + \delta x w_i}\left[\frac{w_{i+1,j} - w_{i,j}}{\delta x e_i} - \frac{w_{i,j} - w_{i-1,j}}{\delta x w_i} \right] + \frac{2}{\delta z_{j+1} + \delta z_j}\left[\frac{w_{i,j+1} - w_{i,j}}{\delta z_{j+1}} - \frac{w_{i,j} - w_{i,j-1}}{\delta z_j} \right]$$

$$[COMPZ]_{i,j} = \frac{2}{\delta z_{j+1+} + \delta z_j}\left(\frac{u_{i,j+1} - u_{i-1,j+1}}{\delta x_i} - \frac{u_{i,j} - u_{i-1,j}}{\delta x_i} \right)$$
$$+ \frac{2}{\delta z_{j+1} + \delta z_j}\left(\frac{w_{i,j+1} - w_{i,j}}{\delta z_{j+1}} - \frac{w_{i,j} - w_{i,j-1}}{\delta z_j} \right) \tag{2.43}$$

$$\left\lfloor \frac{\partial p}{\partial z} \right\rfloor_{i,j} = \frac{p_{i,j+1} - p_{i,j}}{\delta z n_j} \tag{2.44}$$

2.5 Forward Time Discretization of Momentum Equations

Momentum equations that are expressed in equations (2.9) and (2.10) are discretized in time by using forward full time steps in velocity components. Only the next time level, i.e. $(n+1)^{th}$ level is marked, current time levels, i.e $(n)^{th}$ level are not shown with an index.

Pressure terms are at $(n+1/2)^{th}$ time level relative to the velocity components. Instead of considering those indexes for pressure in the formulation, it is preferred to use no index for $(n+1/2)^{th}$ time level and to write "*old*" for $(n-1/2)^{th}$ time level.

So, with the following equations (2.45) and (2.46), horizontal and vertical velocity components are updated.

$$u_{i,j}^{n+1} = u_{i,j} + \delta t \left(g_x + \frac{\mu}{\rho_{i,j}} [LAPLU]_{i,j} + \frac{\mu + \lambda}{\rho_{i,j}} [COMPX]_{i,j} \right)$$
$$- \delta t \left([UDUDX]_{i,j} + [WDUDZ]_{i,j} + \frac{p_{i+1,j} - p_{i,j}}{\delta xe_i} \right) \qquad (2.45)$$

$$w_{i,j}^{n+1} = w_{i,j} + \delta t \left(g_z + \frac{\mu}{\rho_{i,j}} [LAPLW]_{i,j} + \frac{\mu + \lambda}{\rho_{i,j}} [COMPZ]_{i,j} \right)$$
$$- \delta t \left([UDWDX]_{i,j} + [WDWDZ]_{i,j} + \frac{p_{i,j+1} - p_{i,j}}{\delta zn_j} \right) \qquad (2.46)$$

For the sake of simplicity in coding and for defining the same time level expressions in one term, $(n)^{th}$ levels of both x-and z-momentum equations are collected in $F_{i,j}$ and $G_{i,j}$ terms.

$$F_{i,j} = u_{i,j} + \delta t \left(g_x + \frac{\mu}{\rho_{i,j}} [LAPLU]_{i,j} + \frac{\mu + \lambda}{\rho_{i,j}} [COMPX]_{i,j} \right)$$
$$- \delta t \left([UDUDX]_{i,j} + [WDUDZ]_{i,j} \right) \qquad (2.47)$$

24

$$G_{i,j} = w_{i,j} + \delta t \left(g_z + \frac{\mu}{\rho_{i,j}} [LAPLW]_{i,j} + \frac{\mu + \lambda}{\rho_{i,j}} [COMPZ]_{i,j} \right)$$
$$- \delta t \left([UDWDX]_{i,j} + [WDWDZ]_{i,j} \right) \qquad \textbf{(2.48)}$$

Then the next time expressions of horizontal and vertical velocity components become;

$$u_{i,j}^{n+1} = F_{i,j} - \delta t \left(\frac{p_{i+1,j} - p_{i,j}}{\delta x e_i} \right) \qquad \textbf{(2.49)}$$

$$w_{i,j}^{n+1} = G_{i,j} - \delta t \left(\frac{p_{i,j+1} - p_{i,j}}{\delta z n_j} \right) \qquad \textbf{(2.50)}$$

2.6 Forward Time Discretization of Pressure Equation

Up to now velocity components are discretized by using forward time discretization scheme. For the calculation of velocity components' update expressions, i.e. equations (2.49) and (2.50), pressure terms of the next half time step are necessary. This level of pressure can be calculated by using the condition of mass conservation (Eq. 2.8):

The discretization of right hand side of equation (2.8) is:

$$\left(\frac{\partial u}{\partial x} + \frac{\partial w}{\partial z} \right)_{i,j} = \frac{F_{i,j} - F_{i-1,j}}{\delta x_i} + \frac{G_{i,j} - G_{i,j-1}}{\delta z_j} - \frac{\delta t}{\delta x_i} \left[\frac{p_{i+1,j} - p_{i,j}}{\delta x e_i} - \frac{p_{i,j} - p_{i-1,j}}{\delta x w_i} \right]$$
$$- \frac{\delta t}{\delta z_j} \left[\frac{p_{i,j+1} - p_{i,j}}{\delta z n_j} - \frac{p_{i,j} - p_{i,j-1}}{\delta z s_j} \right] \qquad \textbf{(2.51)}$$

and the left hand side is;

$$\frac{\partial p}{\partial t} = \frac{p_{i,j}}{\delta t} - \frac{p_{i,j}^{old}}{\delta t} \qquad \textbf{(2.52)}$$

Then, the continuity becomes;

$$\frac{p_{i,j}}{\delta t} = \frac{p_{i,j}^{old}}{\delta t} - c^2 \frac{F_{i,j} - F_{i-1,j}}{\delta x_i} - c^2 \frac{G_{i,j} - G_{i,j-1}}{\delta z_j} + c^2 \frac{\delta t}{\delta x_i} \left[\frac{p_{i+1,j} - p_{i,j}}{\delta xe_i} - \frac{p_{i,j} - p_{i-1,j}}{\delta xw_i} \right]$$

$$+ c^2 \frac{\delta t}{\delta z_j} \left[\frac{p_{i,j+1} - p_{i,j}}{\delta zn_j} - \frac{p_{i,j} - p_{i,j-1}}{\delta zs_j} \right] \quad \textbf{(2.53)}$$

Equation (2.53) is rearranged to leave the terms at $(n+1/2)^{th}$ time level at the left side;

$$\frac{p_{i,j}}{c^2 \delta t^2} = \frac{p_{i,j}^{old}}{c^2 \delta t^2} - \frac{1}{\delta t}\left[\frac{F_{i,j} - F_{i-1,j}}{\delta x_i} \right] - \frac{1}{\delta t}\left[\frac{G_{i,j} - G_{i,j-1}}{\delta z_j} \right] + \frac{1}{\delta x_i}\left[\frac{p_{i+1,j} - p_{i,j}}{\delta xe_i} - \frac{p_{i,j} - p_{i-1,j}}{\delta xw_i} \right]$$

$$+ \frac{1}{\delta z_j}\left[\frac{p_{i,j+1} - p_{i,j}}{\delta zn_j} - \frac{p_{i,j} - p_{i,j-1}}{\delta zs_j} \right] \quad \textbf{(2.54)}$$

$$\frac{p_{i,j}}{c^2 \delta t^2} - \frac{1}{\delta x_i}\left[\frac{p_{i+1,j} - p_{i,j}}{\delta xe_i} - \frac{p_{i,j} - p_{i-1,j}}{\delta xw_i} \right] - \frac{1}{\delta z_j}\left[\frac{p_{i,j+1} - p_{i,j}}{\delta zn_j} - \frac{p_{i,j} - p_{i,j-1}}{\delta zs_j} \right] = -RHS_{i,j} \textbf{(2.55)}$$

where,

$$RHS_{i,j} = \frac{1}{\delta t}\left[\frac{F_{i,j} - F_{i-1,j}}{\delta x_i} \right] + \frac{1}{\delta t}\left[\frac{G_{i,j} - G_{i,j-1}}{\delta z_j} \right] - \frac{p_{i,j}^{old}}{c^2 \delta t^2} \quad \textbf{(2.56)}$$

Equation (2.55) is rearranged to obtain the expression for $p_{i,j}$;

$$\left[\frac{1}{c^2 \delta t^2} + \frac{1}{\delta x_i \delta xe_i} + \frac{1}{\delta x_i \delta xw_i} + \frac{1}{\delta z_j \delta zn_j} + \frac{1}{\delta z_j \delta zs_j} \right] p_{i,j}$$

$$= \frac{p_{i+1,j}}{\delta x_i \delta xe_i} - \frac{p_{i-1,j}}{\delta x_i \delta xw_i} + \frac{p_{i,j+1}}{\delta z_j \delta zn_j} - \frac{p_{i,j-1}}{\delta z_j \delta zs_j} - RHS_{i,j} \quad \textbf{(2.57)}$$

For the iterative solution of $p_{i,j}$ with Successive Over Relaxation (SOR) method, an expression by using the relaxation parameter ω and the coefficients of $p_{i,j}$ is written;

26

$$\beta = -\left[\dfrac{\varpi}{\dfrac{1}{c^2\delta t^2} + \dfrac{1}{\delta x_i \delta x e_i} + \dfrac{1}{\delta x_i \delta x w_i} + \dfrac{1}{\delta z_j \delta z n_j} + \dfrac{1}{\delta z_j \delta z s_j}}\right] \tag{2.58}$$

The next iteration level of $p_{i,j}$ will be then;

$$p_{i,j}^{iter+1} = (1-\varpi)p_{i,j}^{iter} + \beta RHS_{i,j} - \beta\left[\dfrac{1}{\delta x_i}\left(\dfrac{p_{i+1,j}^{iter}}{\delta x e_i} + \dfrac{p_{i-1,j}^{iter+1}}{\delta x w_i}\right) + \dfrac{1}{\delta z_j}\left(\dfrac{p_{i,j+1}^{iter}}{\delta z n_j} + \dfrac{p_{i,j-1}^{iter+1}}{\delta z s_j}\right)\right] \tag{2.59}$$

Convergence of the PSOR is controlled by using ratio of root mean squares of differences in pressure for each cell between iterations and pressure values. If this ratio gets smaller than 10^{-5}, iteration halts.

$$\dfrac{\sqrt{\sum\limits_{i,j}\left(p_{i,j}^{iter+1} - p_{i,j}^{iter}\right)^2}}{\sqrt{\sum\limits_{i,j}p_{i,j}^{\,2}}} < 10^{-5} \tag{2.60}$$

2.7 Surface Height Method

Variations in the water surface elevation as a result of the bottom movement are to be computed. To do this, "height of fluid" concept is used. Location of the fluid surface information is computed as a function of time. By doing so, one can observe the changes in the height of the fluid in each column of the computational domain. For appropriate treatment, the cell that has the fluid surface is named as the surface cell, below cells are flagged as full cells.

$$\dfrac{\partial h}{\partial t} = w_{surface} - u_{surface}\dfrac{\partial h}{\partial x} \tag{2.61}$$

According to the study of Nichols and Hirt [22], the local velocity, that is the vertical component of the fluid motion plus the horizontal convection of the surface

elevation from the adjacent cell columns, is used in the determination of the surface profile change.

Equation (2.61) is written in finite difference form for variable grid in both *x*- and *z*-directions, using a space centered and forward in time method by adding a positive diffusion term in order to compensate the negative diffusion truncation error as suggested by Nichols and Hirt [22].

$$h_{i,j}^{n+1} = h_{i,j}^{n} + \delta t\left(\overline{w}_{i,j}^{n+1} - [UDHDX]_{i,j}\right) + \frac{2\theta}{\delta xw_i + \delta xe_i}\left(\frac{h_{i+1,j}^{n} - h_{i,j}^{n}}{\delta xe_i} - \frac{h_{i,j}^{n} - h_{i-1,j}^{n}}{\delta xw_i}\right) \quad \textbf{(2.62)}$$

θ is the parameter used for smoothing the numerical solution.

$$1 \geq \theta > \max\left\{\frac{|u_{i,j}|\delta t}{\delta x_i}, \frac{|w_{i,j}|\delta t}{\delta z_j}\right\} \quad \textbf{(2.63)}$$

According to Hirt and Nichols [23], the relation that is given in equation (2.63) should be used by multiplying the right hand side by 1.2 to 1.5.

The vertical velocity component at the free surface is obtained by linear interpolation within the cell,

$$\overline{w}_{i,j}^{n+1} = \frac{\left(h_{i,j}^{n} - z_{j-1}\right)w_{i,j} + \left(z_j - h_{i,j}^{n}\right)w_{i,j-1}}{\delta z_j} \quad \textbf{(2.64)}$$

$$[UDHDX]_{i,j} = \frac{\overline{u}_{i,j}^{n+1}}{\delta x_\alpha}\left(\delta xe_i[DHW]_{i,j} + \delta xw_i[DHE]_{i,j}\right)$$

$$+ \frac{\overline{u}_{i,j}^{n+1}}{\delta x_\alpha}\gamma\,\text{sgn}\left(\overline{u}_{i,j}^{n+1}\right)\left(\delta xe_i[DHW]_{i,j} - \delta xw_i[DHE]_{i,j}\right) \textbf{(2.65)}$$

$$[DHW]_{i,j} = \frac{h_{i,j} - h_{i-1,j}}{\delta x w_i} \tag{2.66}$$

$$[DHE]_{i,j} = \frac{h_{i+1,j} - h_{i,j}}{\delta x e_i} \tag{2.67}$$

$$\overline{u}_{i,j}^{n+1} = \frac{u_{i-1,j}^{n+1} \delta x e_i + u_{i,j}^{n+1} \delta x w_i}{\delta x e_i + \delta x w_i} \tag{2.68}$$

2.7.1 Surface Model

Nichols and Hirt [24] improved free surface boundary conditions. In their study, they suggest a scheme based on a new surface pressure interpolation, which permits the normal stress to be applied at the correct free surface location. Tangential stresses are applied through the assignment of appropriate velocities near the surface.

It is necessary to set boundary conditions by considering mass conservation, normal and tangential stress conditions. With those conditions actual pressure on the surface is treated then the pressure at the center of the surface cell is specified as a linear interpolation (or extrapolation) between the adjacent full cell pressure and the pressure at the fluid surface. A proper cell center pressure is calculated in terms of an interpolation factor, $\eta = \frac{\delta z s_j}{d}$. As can be seen from Fig.2.2, d is the distance from the actual surface to the center of the neighboring full cell.

Then in pressure iterations these quantities are utilized to obtain the next iterated value of the surface cell pressure. Since the distances are calculated according to the actual free surface location, the necessary pressure derivatives are calculated

29

correctly. So, with the surface height formula time wise variation of free surface is calculated.
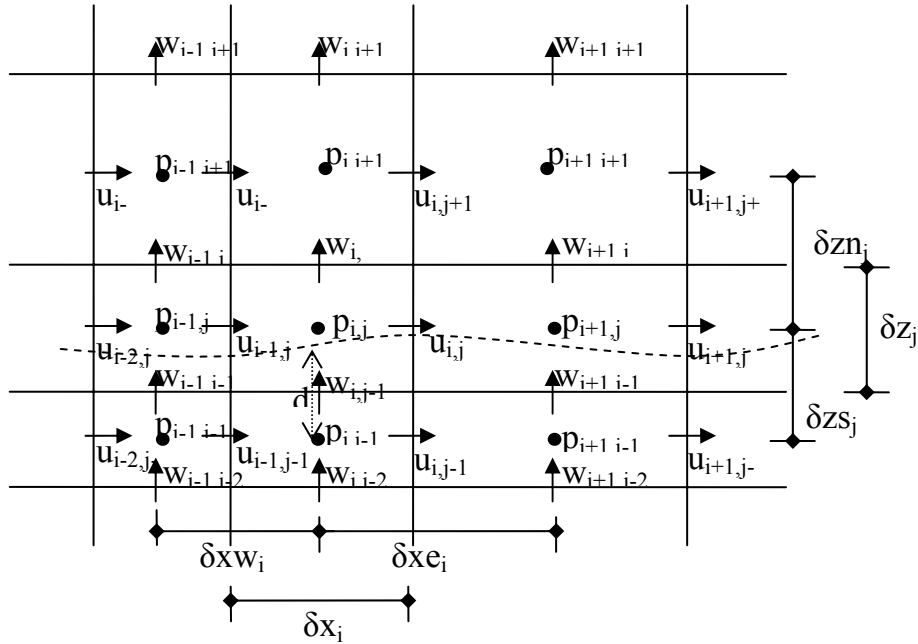

Figure 2.2 Grid and the notation at the free surface

2.8 Bottom Model

The excitation of the system in this study is the rapid movement of the bottom block. To reproduce the correct excitation, it is necessary to provide a continuous motion for the block. For that reason the real location of the moving block is to be followed. The schematic view of the bottom model is seen in Fig 2.3.

The expressions of the model for horizontal and vertical velocities are written by interpolation (or extrapolation) between the known block values and the neighboring full cell values. The vertical velocity component on the block is set as W_{block}, and the horizontal velocity component on the step is zero. Pressure condition is set by writing the normal pressure derivative on the moving block.

The moving block location can be in any place within the grid. Fig 2.4 shows various locations of the block. A constraint must be applied on the bottom model; the block should not move more than one cell in one time step. Initial position coincides with the grid borders.

The distance between the moving bottom and the mesh border is;

$$d = \delta z_j - base_i \tag{2.69}$$

where $base_i$ is the location of the moving bottom in meters.
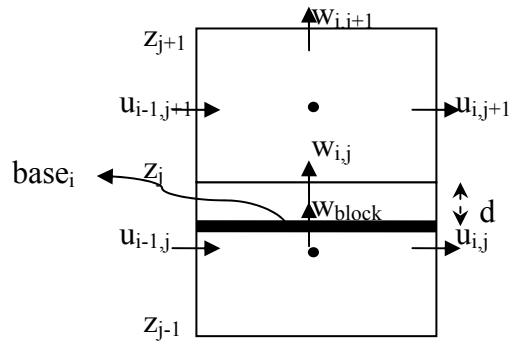
Figure 2.3 Bottom model
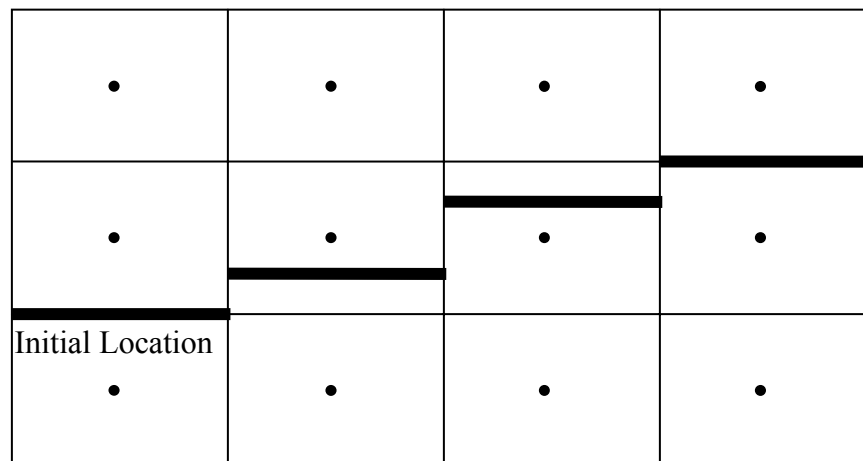
Figure 2.4 Various locations of the block

2.9 Boundary Conditions

Boundary conditions are the statements that are used to describe the real system to the mathematical model. In this study, the computational domain has various boundaries, such as fixed wall, moving wall, no-reflection, free surface and symmetry (Fig.2.5). To reduce computational costs, by using the symmetry property half of the domain is solved.
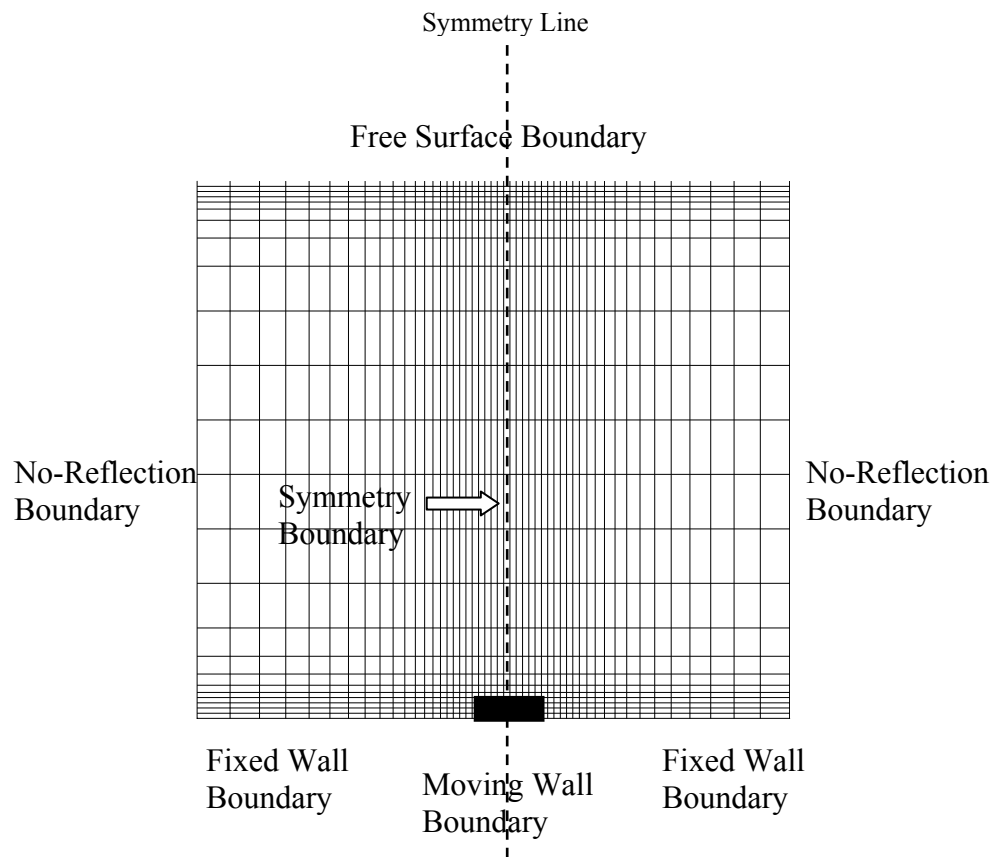

Figure 2.5 Boundary conditions

2.9.1 Fixed Wall Boundary

No-slip condition is utilized for the fixed wall sections of the computational domain. Since in staggered grid system vertical velocity components are defined on the boundary, they are set to zero for fixed wall sections. For pressure boundary condition simply hydrostatic case is considered.

$$u_{i,1} = -u_{i,2} \tag{2.70}$$

$$w_{i,1} = 0 \tag{2.71}$$

$$p_{i,1} = p_{i,2} - g_z \delta z_2 \tag{2.72}$$

2.9.2 Moving Wall Boundary

In this study the mid portion of the bottom side is moving for a few seconds. Horizontal velocity components are suitable for no-slip condition since there is not a horizontal bottom motion. Besides the vertical velocity component is calculated by considering the block velocity to reflect the block motion to the numerical solution. Since the pressure change will be significant for this portion of the bottom side, it is preferred to write a more precise boundary condition by considering the normal derivative of the pressure. To write the normal pressure derivative, fictitious vertical velocity, w_0, is necessary.

$$u_{i,j} = -u_{i,j+1} \left[\frac{\left(\frac{\delta z_j}{2} - d \right)}{\left(\frac{\delta z_{j+1}}{2} + d \right)} \right] \tag{2.73}$$

$$w_{i,j} = w_{i,j+1} + \delta z_{j+1} \frac{\left(w_{step} - w_{i,j+1} \right)}{\left(\delta z_{j+1} + d \right)} \tag{2.74}$$

$$w_o = \frac{\left(\delta z_{j+1} + \delta z_j\right)\left[w_{i,j+2} - 3w_{i,j+1} + 3w_{i,j}\right] - 6\delta z_{j+2} w_{i,j+1}}{\delta z_{j+1} + \delta z_j - 6\delta z_{j+2}} \tag{2.75}$$

$$p_{i,j} = p_{i,j+1} - \delta z n_j \mu \left[\frac{w_{i,j+1} - 2w_{i,j} + w_o}{\delta z_{j+1} \delta z_j}\right] + \delta z n_j g_z \tag{2.76}$$

2.9.3 Fixed Side Wall Boundary

Side walls of the moving bottom portion should be considered separately. For that section horizontal velocities coincide with the boundary, so, because of the fact that there is no motion in horizontal direction they are set to zero. For the vertical velocity components no-slip condition is valid. Here the pressure boundary conditions are written by equating the horizontal gradients of pressure terms to zero.

$$u_{NS-1,j} = 0 \tag{2.77}$$

$$w_{NS,j} = -w_{NS-1,j} \tag{2.78}$$

$$p_{NS,j} = p_{NS-1,j} \tag{2.79}$$

2.9.4 No-Reflection Boundary

Right and left sides of the computational domain are considered as no-reflection boundaries. Only the left half of the domain is solved, right is computed by symmetry. The conditions for the left side are given below. For this boundary, horizontal gradients of the dependent variables are set to zero.

$$u_{1,j} = u_{2,j} \tag{2.80}$$

$$w_{1,j} = w_{2,j} \tag{2.81}$$

$$p_{1,j} = p_{2,j} \tag{2.82}$$

2.9.5 Symmetry Boundary

To reduce computational costs and memory allocation, half of the domain is solved. In every iteration, values calculated for the left half domain is copied to the right. Effectively on the boundary following equations are satisfied.

$$u_{\frac{N+1}{2},j} = 0 \tag{2.83}$$

$$w_{\frac{N+3}{2},j} = w_{\frac{N+1}{2},j} \tag{2.84}$$

$$p_{\frac{N+3}{2},j} = p_{\frac{N+1}{2},j} \tag{2.85}$$

2.9.6 Free Surface Boundary

Since wave height is relatively small compared to the length of the wave, nearly horizontal surface can be assumed while deriving the free surface boundary conditions [24].

$$\sigma_{zz} = -p + 2\left(\frac{\mu}{\rho}\right)\frac{\partial w}{\partial z} = 0 \tag{2.86}$$

$$\tau_{zx} = \left(\frac{\mu}{\rho}\right)\left[\frac{\partial u}{\partial z} + \frac{\partial w}{\partial x}\right] = 0 \tag{2.87}$$

Then, normal stress condition is:

$$p = 2\left(\frac{\mu}{\rho}\right)\frac{\partial w}{\partial z} \tag{2.88}$$

and tangential stress condition is:

$$\frac{\partial u}{\partial z} + \frac{\partial w}{\partial x} = 0 \tag{2.89}$$

From the continuity and the tangential stress condition, the normal and tangential velocity components are computed as:

$$w_{i,j} = w_{i,j-1} - \frac{\delta z_j}{\delta x_i}\left(u_{i,j} - u_{i-1,j}\right)$$ (2.90)

$$u_{i-1,j+1} = u_{i-1,j} - \frac{\delta z n_j}{\delta x w_i}\left(w_{i,j} - w_{i-1,j}\right)$$ (2.91)

Pressure on the free surface is computed from the normal stress condition:

$$p_{surface} = 2\left(\frac{\mu}{\rho_{i,j}}\right)\left|\frac{w_{i,j} - w_{i,j-1}}{\delta z_j}\right|$$ (2.92)

The interpolation factor η is defined as:

$$\eta = \frac{\delta z s_j}{d}$$ (2.93)

Then the pressure at the cell center is calculated from:

$$p_{i,j} = \eta p_{surface} + (1 - \eta)p_{i,j-1}$$ (2.94)

2.10 Stability Conditions

Since numerical solutions are not as exact as the analytical solutions, the former always have instability problem. In order to ensure stability of the numerical computations and avoid generating oscillations, stability conditions must be imposed on the mesh sizes δx and δz, and time step size δt [16].

$$\delta t < \min\left\{\frac{\delta x_i}{|u_{i,j}|}, \frac{\delta z_j}{|w_{i,j}|}\right\}$$ (2.95)

Equation (2.95) gives the Courant-Friedrichs-Lewy (CFL) condition. According to this statement, after selecting sufficiently small mesh dimensions and assuming there exists fluxes only between adjacent cells, no fluid particle may travel a distance greater than the mesh spacing δx or δz in time δt. In their study, Hirt and Nichols [23] suggest that using one fourth to one third of the minimum time increment makes the solution more stable.

For viscous flows, momentum must not diffuse more than approximately one cell in time δt [23]. This statement can be expressed as;

$$\delta t < \frac{\mu}{2\rho_{i,j}} \left[\frac{1}{\delta x_i^2} + \frac{1}{\delta z_j^2} \right]^{-1} \tag{2.96}$$

CHAPTER III

COMPUTATIONAL TESTS

3.1 Computational Domain

To apply the mathematical model that is described in the second chapter, a hypothetical domain (Fig.1.2) is considered. Various values of L_R, H, H_S and L_S are used.

It is necessary to model the motion as a rapid one. According to the study of Tyvand, et al. [13], the impulsive bottom deflection should have a duration shorter than the gravitational time, $(h/g)^{1/2}$. Here h is the ocean depth which is assumed to be constant initially, and g is the gravitational acceleration. Therefore, with the above parameters selected in this study, completion of the block motion in approximately several seconds can be considered as rapid.

3.2 Grid Resolution Check

In numerical solutions, resolution of the computational domain should be fine enough to model the physical system accurately. Therefore, decision of the grid ratios is important. Since by doing so, one can control the grid distribution better, such that, the regions where physical quantities change rapidly, can be expressed with finer mesh.

For this numerical solution, it is decided to use a computational domain that has the maximum mesh size in x-direction in right and left far fields, minimum mesh size of

that direction in the mid part, which covers the moving block. In *z*-direction, the minimum mesh size is utilized in both upper and lower parts of the domain, which covers both moving block and the surface waves, and the maximum mesh size is used in the mid part. (Fig. 3.1)
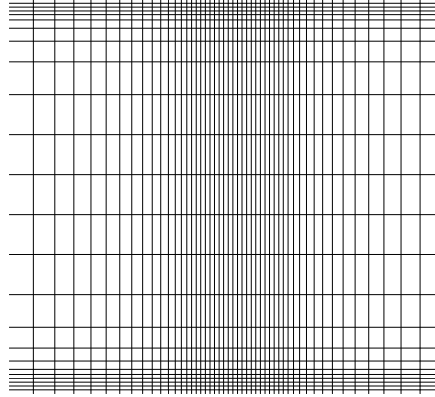

Figure 3.1 Computational mesh

Apart from the variable grid distribution, the number of computational nodes has direct effect on the grid resolution. With a less number of nodes, one may get wrong results. However, using more than the sufficient number of nodes, increases the computational time and makes the numerical solution inefficient. To decide on the sufficient number of nodes, different NxM values are studied, and the results are checked with the most important parameter of this study, the maximum water height, h_{max}. During this check a constant ratio between N and M values, that is 2:1, is used according to the results of Kırlangıç [15].

Variables that are used to construct the computational mesh can be seen in Fig 3.2. The clustering relations are selected under the light of the study of Kırlangıç [15].
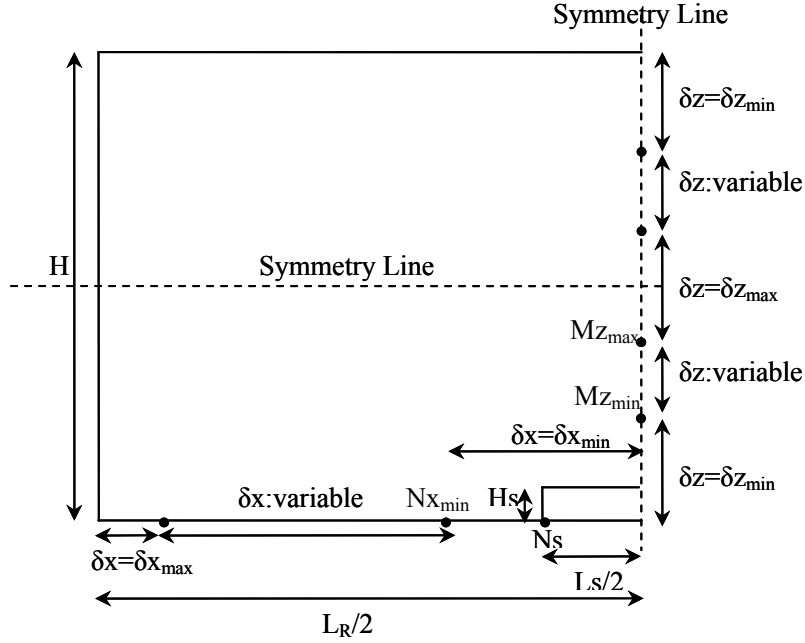
Figure 3.2 Mesh variables

Nx_{min} shows number of the cell from which the constant minimum mesh size in x-direction starts. Ns represents the node where the moving block starts. L values show the length of the corresponding nodes from the initial point. β values show the clustering ratio in the corresponding direction. Mz_{min} shows the end of the constant minimum mesh size in z-direction level in terms of nodal point. In addition, Mz_{max} represents number of the cell from which the constant maximum mesh size in z-direction starts. The computational mesh is symmetric with respect to the mid lines of x and z directions. For all grid cases, the height of point Mz_{min} is taken to be 2.5xH_S and the distance between point Nx_{min} and vertical symmetry line is taken to be L_S. The details of grid data for different NxM selections are shown in Table 3.1;

Table 3.1 Detailed Grid Alternatives for Grid Resolution Check

NxM	51x25	101x51	151x75	251x125	401x201	501x251	601x301	701x351
Number of Nodes	1275	5151	11325	31375	80601	125751	180901	246051
Nx_{min}	14	30	38	79	110	151	170	193
$L(Nx_{min})(m)$	400.27	400.75	400.59	400.365	400.238	400.411	399.58	399.42
Ns	21	40	57	103	156	201	236	273
$L(Ns)(m)$	454.66	448.01	450.29	451.24	450.667	450.205	450.17	450.349
β_x	0.861	0.9393	0.9387	0.9803	0.9813	0.9886	0.9886	0.9895
δx_{min} (m)	9.0662	4.726	2.615	2.11	1.096	0.9958	0.766	0.6365
δx_{max} (m)	63.443	29.0517	27.17	10.00	8.58	5.56	5.32	4.83
Mz_{min}	5	8	10	13	40	50	70	33
$L(Mz_{min})(m)$	5.081	5.004	5.005	4.9997	5.051	4.937	4.92	5.089
Mz_{max}	10	18	26	38	81	100	120	98
$L(Mz_{max})(m)$	24.34	22.83	24.599	23.19	25.95	25.079	22.093	21.873
β_z	0.7167	0.861	0.9193	0.961	0.9461	0.955	0.9499	0.9864
δz_{min} (m)	1.272	0.7148	0.5561	0.4166	0.129	0.10	0.0713	0.159
δz_{max} (m)	9.3858	3.7084	2.3250	1.172	1.3274	1.054	0.9808	0.3926

The relation between the number of nodes and the maximum water height is shown in Fig. 3.3;
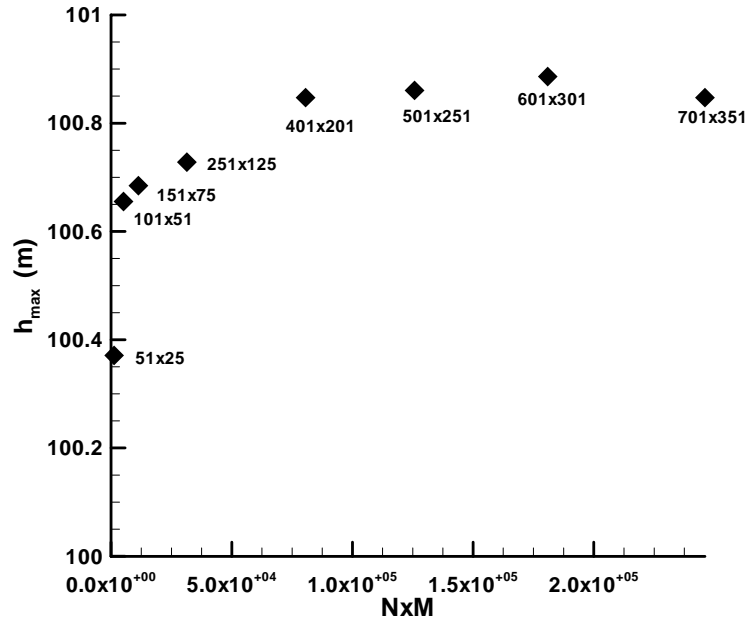
Figure 3.3 h_{max} versus NxM for grid resolution check

As can be seen from Fig. 3.3, as the number of nodes increases, h_{max} increases. After 401x201, h_{max} value does not change much. Indeed, after 601x301, h_{max} value has tendency to decrease. This is because of the round-off errors. When the mesh becomes finer, there is the danger of error accumulation. Therefore, to obtain a solution with minimum round-off error and to save the computational time it is preferred to use 501x251 nodes.

3.3 Far Field Boundary Condition Check

In all numerical studies, boundary conditions are the constraints of the system and they help the convergence of the solution to the real situation. In this study, it is

important to impose a correct boundary condition at the far field side. Since a large domain is solved numerically, one does not want to get any reflections from the far field boundary. For that purpose the system is solved with two different boundary conditions to observe their effect to the time history of water height of the column on the symmetry line, $h_0(t)$. In the first case, far field boundary conditions of velocities, pressure and free surface are set as the ones that make the first derivatives of the corresponding one to zero. In the second run, the second derivatives are set to zero.
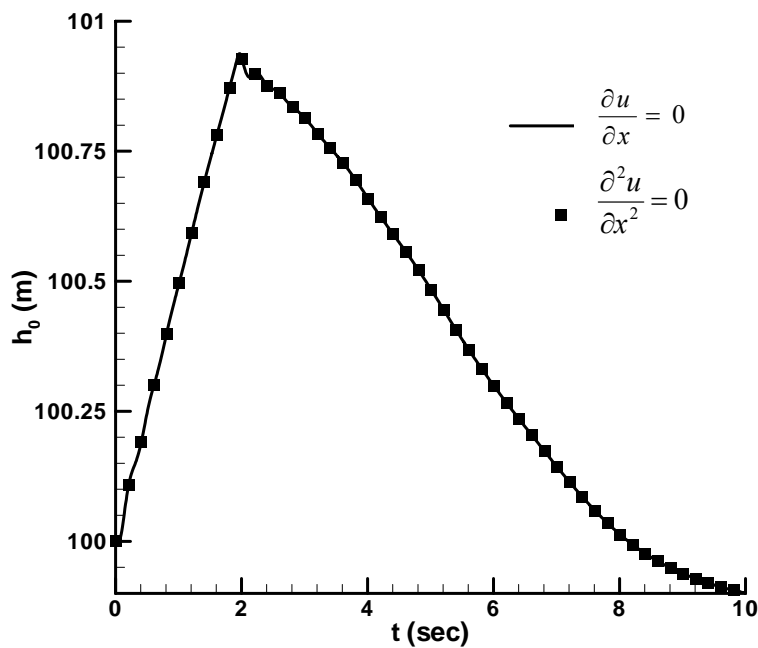
Figure 3.4 h_0 versus t to check the effects of far field boundary conditions

As can be seen from Fig. 3.4, there is not any difference between the first and second cases, both graphs coincide on each other. It is preferred to set boundary conditions by considering the degree of the governing equation, which is by taking one degree less for boundary conditions. Since the equation that is utilized to form

43

the mathematical model is a second order differential equation, it is decided to set the first derivatives of velocities, pressure and free surface to zero in the far field.

3.4 How Far Should be the Far Field Boundary?

Computational domain should be large enough to supply no-reflection boundary to the system. To check whether the domain length is large enough or not, different L_R values are tested and the results of each run are presented. Again the controlling criterion is the time history of water height of the column on the symmetry line, $h_0(t)$. Water depth, H; step height, H_S; step length, L_S; and number of nodes, NxM values in each run are set to be constant, i.e. 100m, 2 m, 100 m and 501x251 respectively.

The resulting plot which gives the relation between L_R and h_0 is shown in Fig.3.5;
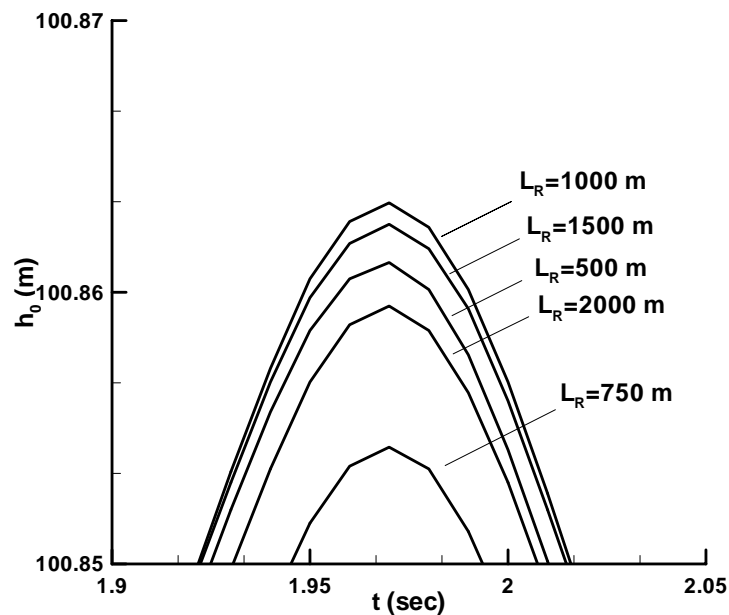
Figure 3.5 h_0 versus t for different L_R values

As can be seen from Fig. 3.5 computational domains with L_R values that are less than 10xH, are affected from the boundaries since they are not large enough. The maximum h_0 is less than the one obtained for L_R=10xH=1000 m. On the other hand, in computational domains with L_R values greater than 1000 m, grid resolution problem is seen. Since for large domains, with the same number of nodes, grid resolution reduces; $(h_0)_{max}$ is again less than the one obtained for 1000m.

Domain length is a function of water depth and block length. Therefore, relations of L_R with both L_S and H should be checked separately. Then the maximum L_R value should be utilized. According to the results obtained by this computational test, L_R=10xH relation is selected for the model.

3.5 Dissipation Check

For determination of free surface profiles, time dependent variation of water height is computed. According to the study of Nichols and Hirt [22], it is necessary to use a positive diffusion term to compensate the negative diffusion due to truncation error. In their research they solved a water tank which is small in size compared to the computational domain in this study. In the present problem the computational domain is so big and the surface deformations are relatively small. Therefore, it is necessary to try different dissipation coefficients to see the requirement of that additional dissipation term of Nichols and Hirt [22] in the free surface equation.

As can be seen from Fig. 3.6 both full dissipation and no dissipation graphs coincide. Therefore, it is decided that, for this study additional dissipation term is not necessary.
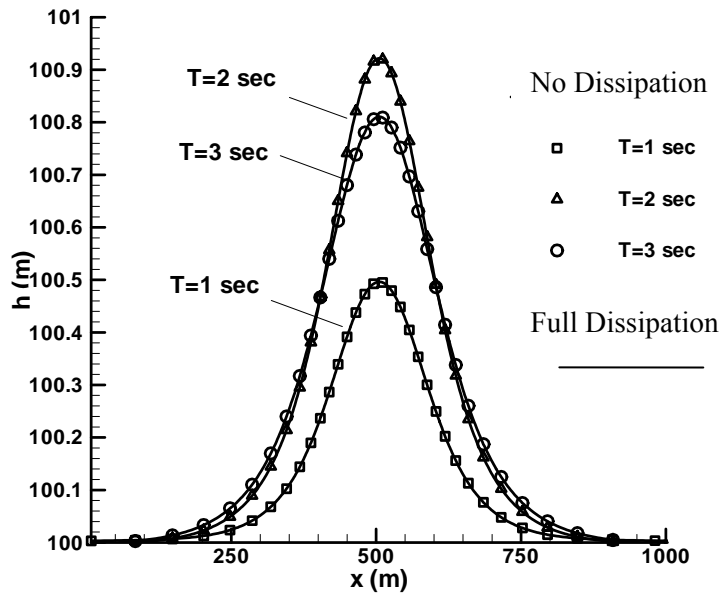
Figure 3.6 *h* versus *x* graph to check the dissipation term effect

3.6 Block Velocity

The excitation of the hydrostatic fluid is given by the sudden block movement on the sea bed. Moving the block at a constant velocity causes very large accelerations at the start of the motion and very large decelerations at the end of the motion. Large decelerations at the end of the motion of the block produces very sharp pressure fluctuations on the surface of the moving block which may not be the case in a natural crack formation at the sea bed.

In nature, it may take some time to reach the maximum velocity from stationary position and some time to reduce velocity from maximum value to zero, such that the accelerations and decelerations are finite. Therefore, variable velocity for the block motion is considered to eliminate any unrealistic start and stop disturbances

46

on the flow field. To investigate the effect of block velocity variations on the surface waves, velocity and pressure fields, three points A, B and C on the symmetry line are selected (Fig. 3.7). Point A is at the midway between the initial and final configurations of the moving block. Point B is just at the final position of the block and point C is always above the moving block. The distance between B and C is only a vertical mesh size.
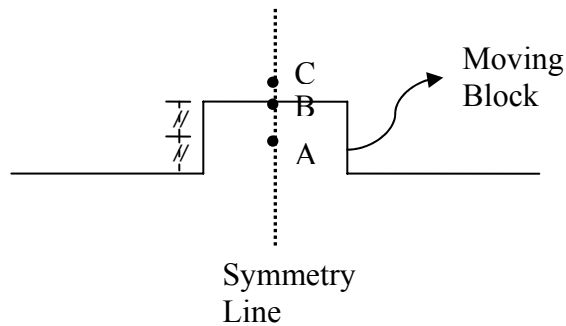

Figure 3.7 Observation points on the symmetry axis

With maximum block velocity of 1 m/s, block height of 2 m and no smoothing in accelerating and decelerating stages, the plots of vertical velocity and pressure at points A, B and C are shown in Figs. 3.8 and 3.9. When the block stops at t = 2 seconds, a large pressure wave is created at point C (Fig. 3.9). It is also noticed that this pressure wave due to sudden deceleration influences the surface deformations.
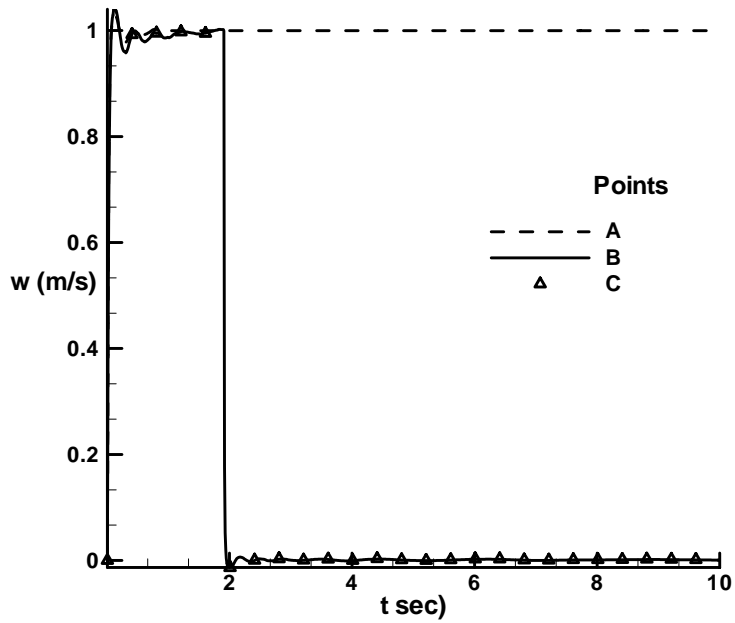
**Figure 3.8** *w* versus *t* for points A, B and C (No smoothing)
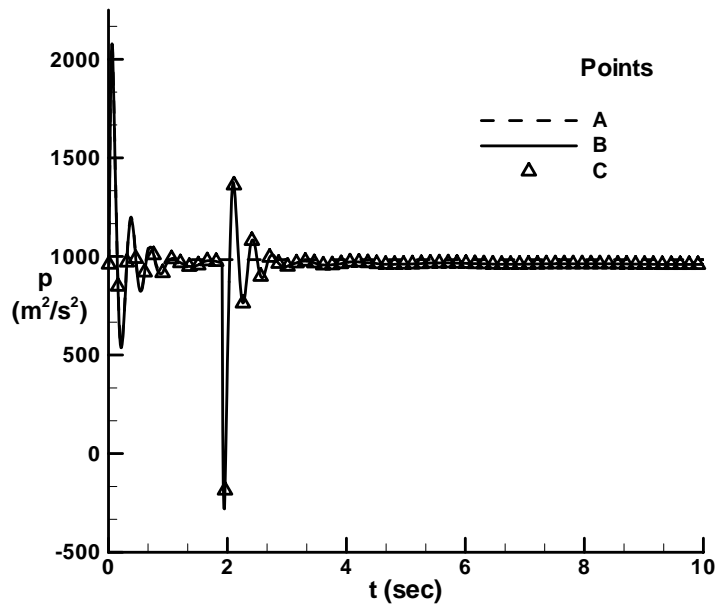
Figure 3.9 *p* versus *t* for points A, B and C (No smoothing)

Since point A is at the midway between the initial and final configurations of the moving block, after the block passes it, it will be out of the computational domain. Therefore, vertical velocity and pressure values of that point do not change. Due to the fact that point B and C are so close to each other their graphs coincide.

To see the effect of block velocity variations, time dependent variations of vertical velocity and pressure at points A, B and C are examined. To do this, velocity of the moving block is assumed to have three stages; acceleration stage, constant maximum velocity and deceleration stage (Fig. 3.10).
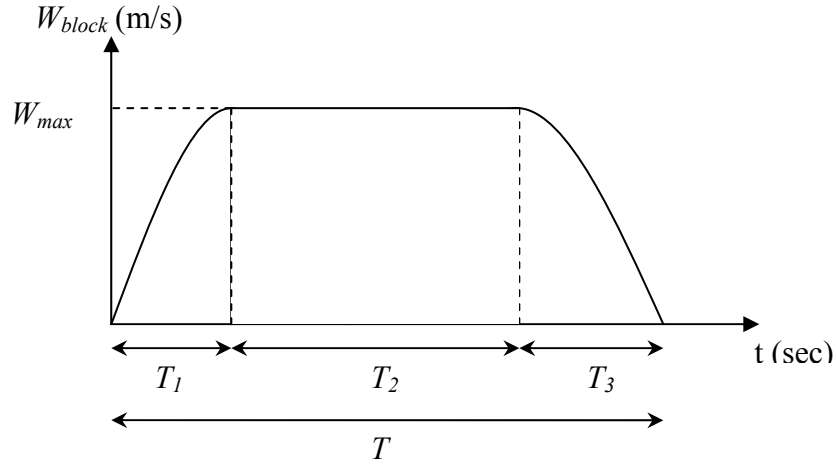
Figure 3.10 Velocity histogram for the moving block

For accelerating stage, $(0 < t \leq T_1)$:

$$W_{block} = W_{max} Sin\left(\frac{t}{T_1}\frac{\pi}{2}\right) \tag{3.1}$$

For constant maximum velocity stage, $(T_1 < t \leq T_1 + T_2)$:

$$W_{block} = W_{max} \tag{3.2}$$

For deceleration stage, $(T_1 + T_2 < t \leq T)$:

$$W_{block} = W_{max} \, Sin\left(\frac{(t - T_1 - T_2)}{T_3}\frac{\pi}{2} + \frac{\pi}{2}\right)$$ (3.3)

where t : time (sec)

   T_1 : period of acceleration (sec)

   T_2 : period of constant velocity (sec)

   T_3 : period of deceleration (sec)

The relation between T_1, T_2 and T_3 are written with respect to the total motion duration T as;

$$T_1 = k_1 T$$ (3.4)

$$T_3 = k_3 T$$ (3.5)

$$T_2 = T - T_1 - T_3$$ (3.6)

By using the equations (3.4) and (3.5) the expression for T_2 becomes;

$$T_2 = T - (k_1 T + k_3 T)$$
$$= T[1 - k_1 - k_3]$$ (3.7)

Then total duration of motion and the expressions for the durations of velocity increasing and decreasing sections becomes;

$$T = \frac{T_2}{[1 - k_1 - k_3]}$$ (3.8)

$$T_1 = k_1 \frac{T_2}{[1 - k_1 - k_3]}$$ (3.9)

$$T_3 = k_3 \frac{T_2}{[1 - k_1 - k_3]}$$ (3.10)

The expression for T_2 is derived by considering the criteria that the area under the velocity histogram is equal to the step height, Hs;

$$Area = A_1 + A_2 + A_3 \tag{3.11}$$

$$A_1 = \int_0^{T_1} W_{max} Sin\left(\frac{t}{T_1}\frac{\pi}{2}\right) dt = W_{max} \int_0^{\frac{\pi}{2}} Sin(u)\frac{2T_1}{\pi} du$$

$$= W_{max} \frac{2T_1}{\pi}(-Cos(u))\Big|_0^{\frac{\pi}{2}} = W_{max} \frac{2T_1}{\pi} \tag{3.12}$$

where $u = \dfrac{t}{T_1}\dfrac{\pi}{2}$ and $du = \dfrac{\pi}{2T_1} dt$

$$A_3 = \int_{T_1+T_2}^{T_1+T_2+T_3} W_{max} Sin\left(\frac{t-T_1-T_2}{T_3}\frac{\pi}{2}+\frac{\pi}{2}\right) dt$$

$$= W_{max} \int_{T_1+T_2}^{T_1+T_2+T_3} Cos\left(\frac{t-T_1-T_2}{T_3}\frac{\pi}{2}\right) dt = W_{max} \frac{2T_3}{\pi} \tag{3.13}$$

$$H_S = W_{max}\frac{2T_1}{\pi} + W_{max}T_2 + W_{max}\frac{2T_3}{\pi} \tag{3.14}$$

$$\frac{H_S}{W_{max}} = \frac{2}{\pi}(T_1 + T_3) + T_2 \tag{3.15}$$

$$\frac{H_S}{W_{max}} = \frac{2}{\pi}\left[k_1 \frac{T_2}{(1-k_1-k_3)} + k_3 \frac{T_2}{(1-k_1-k_3)}\right] + T_2 \tag{3.16}$$

$$\frac{H_S}{W_{max}} = \frac{2}{\pi(1-k_1-k_3)}(k_1 + k_3)T_2 + T_2 \tag{3.17}$$

$$T_2 = \frac{\dfrac{H_S}{W_{max}}}{\left[\dfrac{2(k_1 + k_3)}{\pi(1 - k_1 - k_3)} + 1\right]} \tag{3.18}$$

In order to examine the effects of accelerating and decelerating stages separately on the time history of water height of the column on the symmetry line, h_0, various accelerating and decelerating stage coefficients are tested.

Table 3.2 Various accelerating stages

k_1	0	0.05	0.1	0.2
k_3	0	0	0	0

At first, various acceleration periods are considered (Table 3.2) with a sudden deceleration. Velocity of the moving block with these configurations and the corresponding time histories of water height of the column on the symmetry line are shown in Fig. 3.11 and Fig. 3.12;
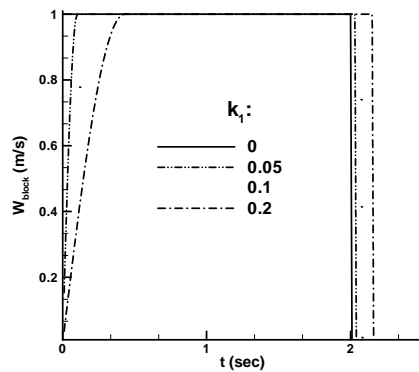
Figure 3.11 W_{block} versus t for different k_1 values
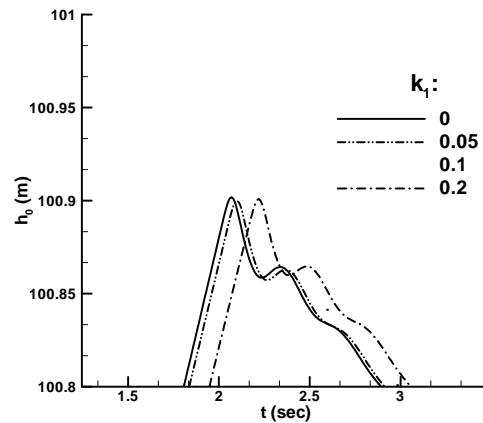
Figure 3.12 h_0 versus t for different k_1 values

52

It is seen that different k_1 values only cause time lag of the h_0 values. Therefore, it is preferred to use $k_1 = 0$, since smoothing of the accelerating stage does not affect the form and amplitude of the surface waves.

To examine the effects of decelerating stage to the time history of h_0, various deceleration configurations are tested (Table 3.3).

**Table 3.3** Various decelerating stages

k_1	0	0	0	0	0
k_3	0	0.1	0.25	0.3	0.5
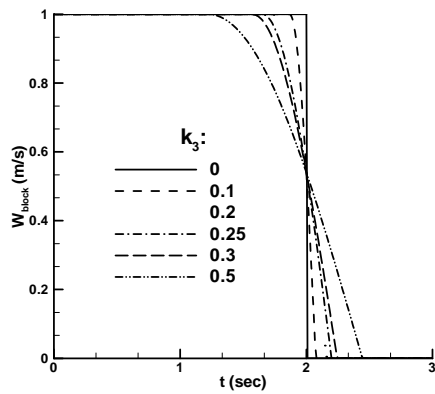
Figure 3.13 W_{block} versus t for different k_3 values
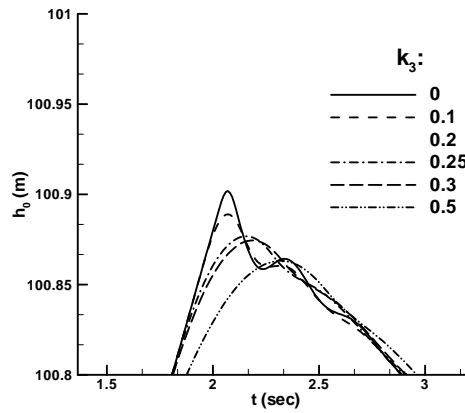
Figure 3.14 h_0 versus t for different k_3 values

As can be seen from Figs. 3.13 and 3.14, as the duration of the decelerating stage increases, resulting h_0 graph becomes smoother with a reduced $(h_0)_{max}$. When 25% of the total motion duration is utilized for the decelerating stage, it is sufficient for secondary damp effect smoothing. Therefore, it is decided to use $k_3 = 0.25$.

With maximum block velocity of 1 m/s, block height of 2 m and the decided decelerating stage, the plots of vertical velocity and pressure for points A, B and C are shown in Figs. 3.15 and 3.16;
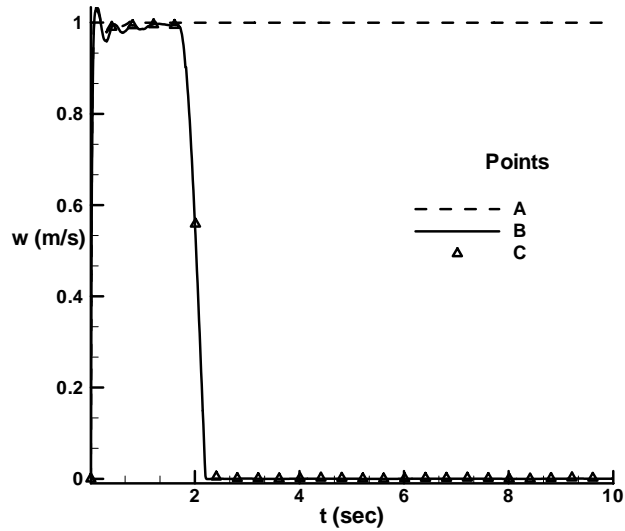

Figure 3.15 *w* versus *t* for points A, B and C (Deceleration stage smoothing)
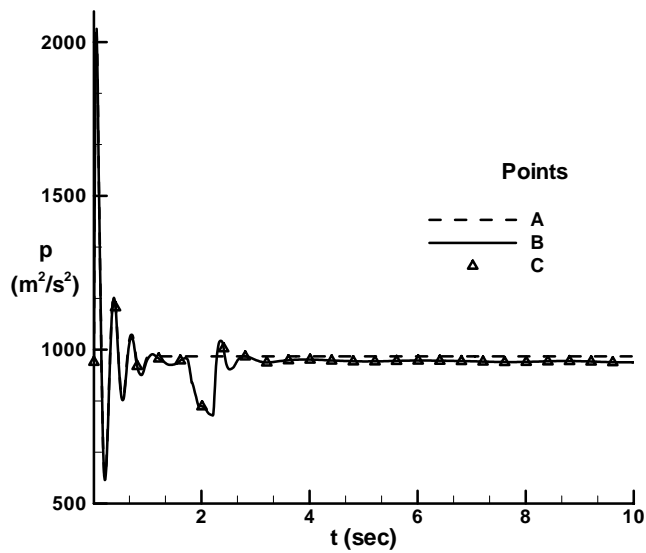

Figure 3.16 *p* versus *t* for points A, B and C (Deceleration stage smoothing)

From Fig. 3.16 it is seen that, as the duration of the decelerating stage increases, the secondary pressure wave is reduced.

It is also necessary to check for the maximum block velocity sufficient to obtain a rapid motion. For that purpose various maximum velocities are tested and their effects on the time histories of h_0 are discussed.
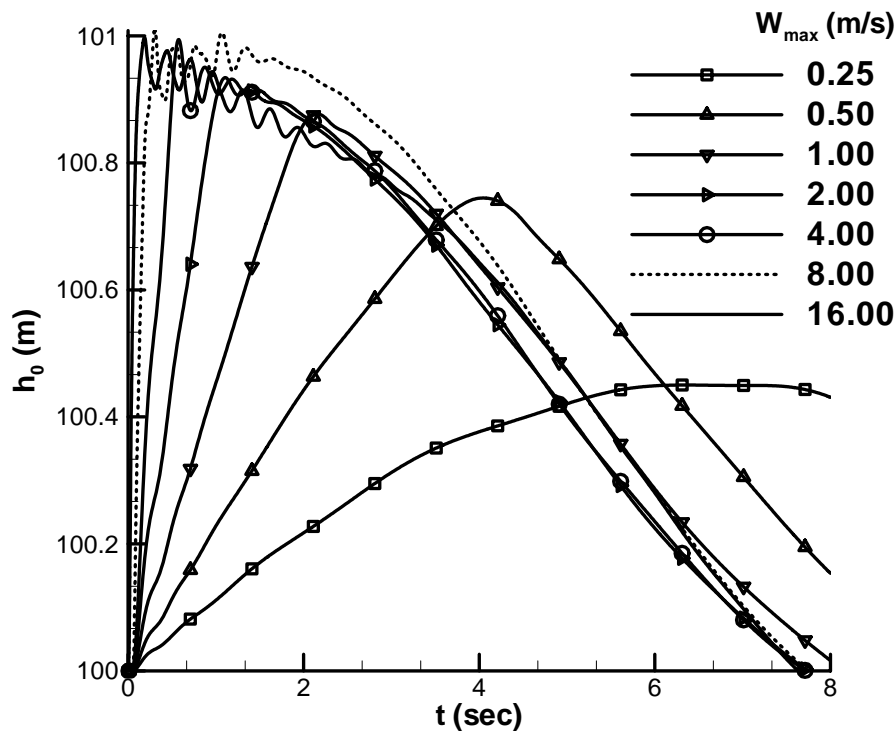

Figure 3.17 h_0 versus t for different maximum block velocities

From Fig. 3.17 it is seen that maximum block velocity values of 4, 8 and 16 m/s are close to each other. The differences on their values cause time lag and small variations in the maximum values of h_0. Since the difference is small, it is decided to use W_{max} =4 m/s as the maximum block velocity.

CHAPTER IV

EXAMPLE SOLUTIONS

4.1 General

In the previous chapters, mathematical model was constructed and computational parameters were tested. In the tests, the hypothetical domain parameters were also kept constant. In nature, ocean depth is varying in the region. Therefore it is not appropriate to fix a certain value for water depth, H. Besides, it is difficult to determine a fault crack dimensions.

For the system of this study, step length L_S, its height H_S, water depth of the domain, H and its length, L_R are the input parameters. So, to examine their effects on the maximum water height, various cases can be studied.

4.2 Relation between h_{max}, H and H_S

With the previous computational tests a relation is determined to express domain length L_R in terms of water height, H and step length, L_S. According to that relation it is necessary to use the maximum L_R value that is obtained from the relations $L_R=10 \mathrm{x} H$ and $L_R=10 \mathrm{x} L_S$. In addition, from the tests on the block velocity, it is decided to use smoothing in decelerating stage to reduce the secondary damp effect, which is not so natural. According to those tests, to obtain the maximum water height and to give the block a rapid rise, it is necessary to use maximum block velocity of, $W_{max}=4$ m/s.

Since $h_{max} =f~(H, H_S)$, by using those results, the effects of various H and H_S combinations on the maximum water height is examined (Table 4.1).

Table 4.1 Maximum water height for various H and H_S combinations

| H_S (m)\ H (m)	100	1000
1	100.526	1001.13
2	100.994	1001.96
4	101.888	1003.31
6	102.781	1004.19
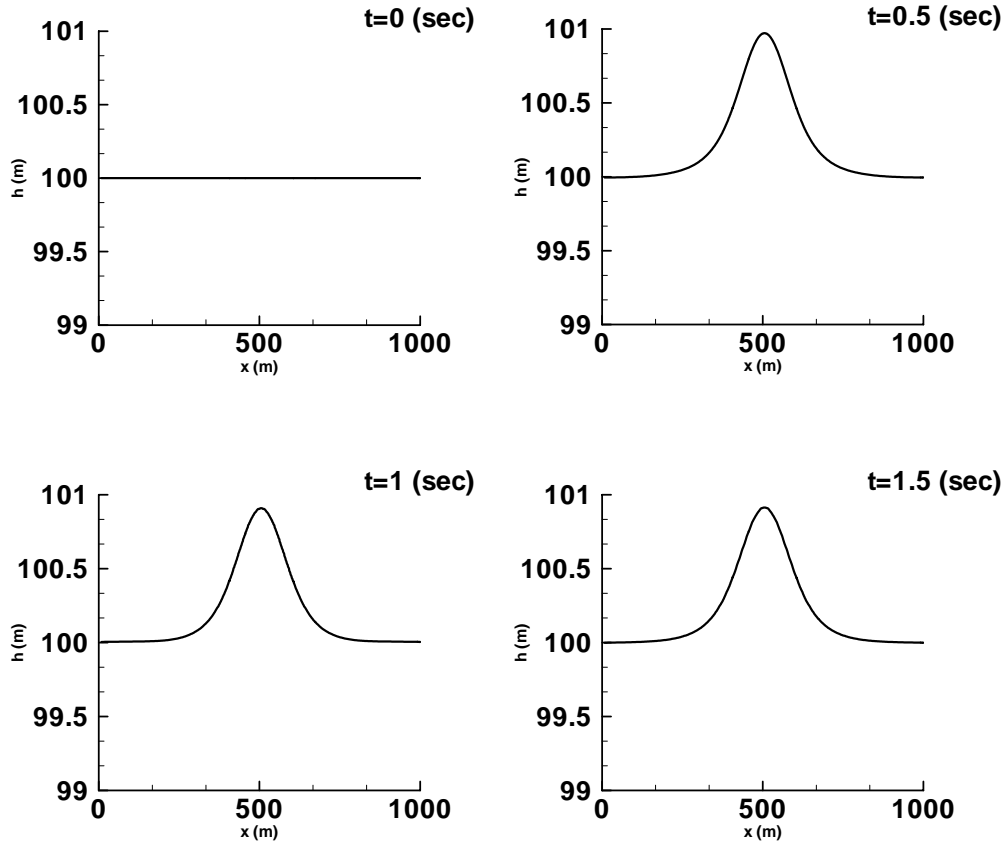
Figure 4.1 Free surface profiles for H = 100 m and H_S = 2 m
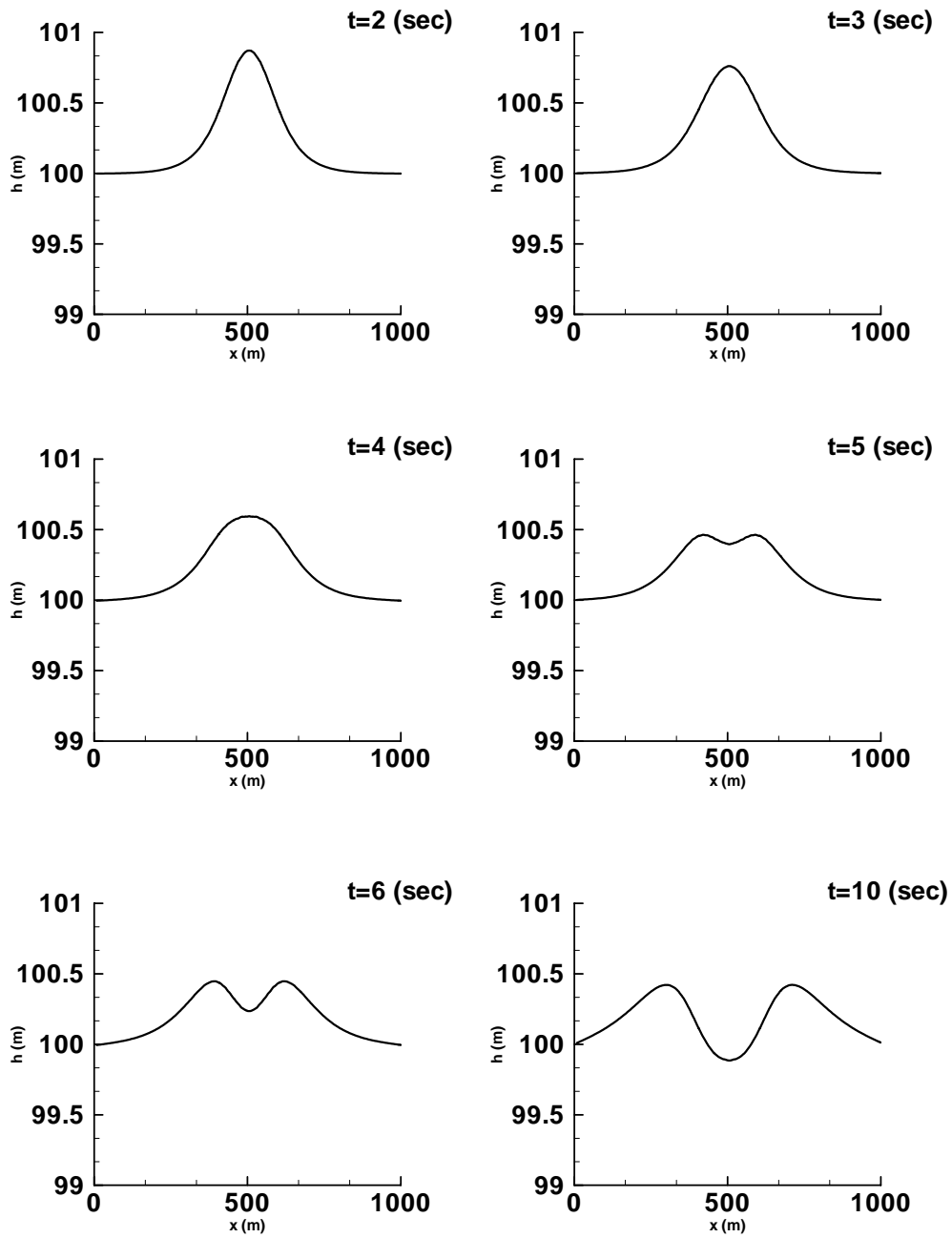
Figure 4.1 (continued)
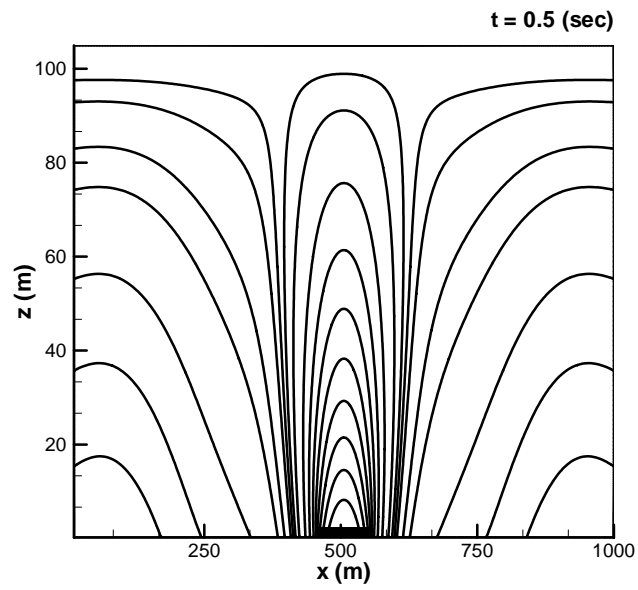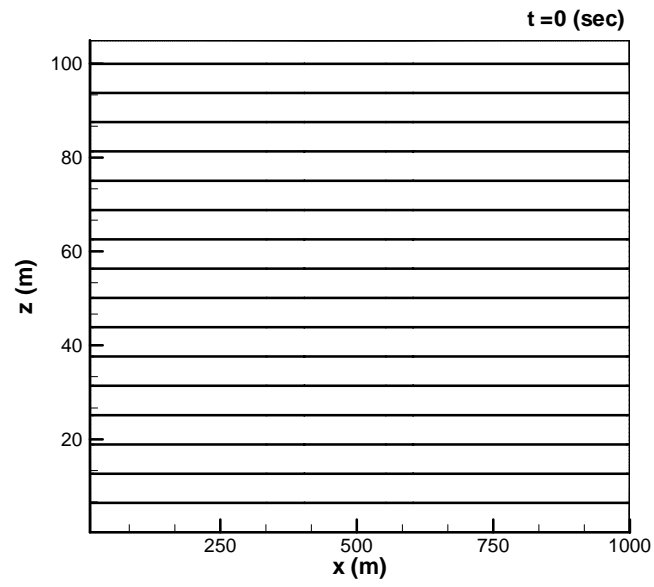
Figure 4.2 Pressure fields for H = 100 m and H_S = 2 m

t=1 (sec)

**t = 1.5 (sec)**

Figure 4.2 (continued)

60
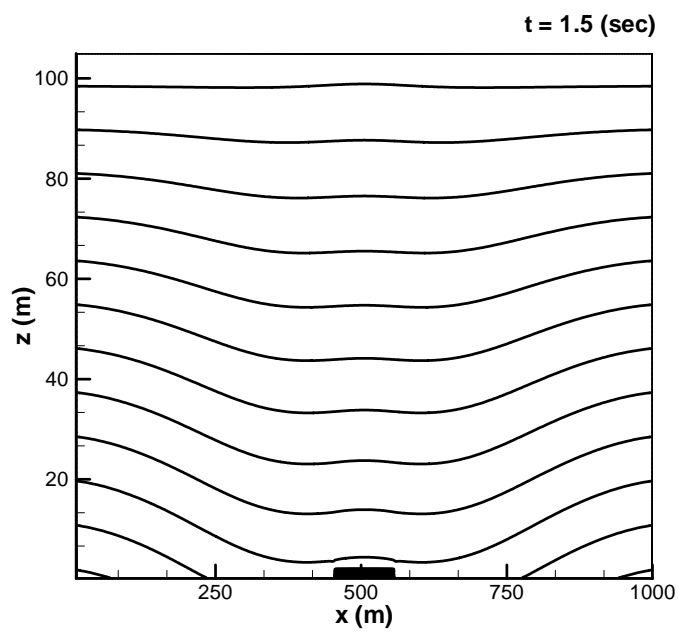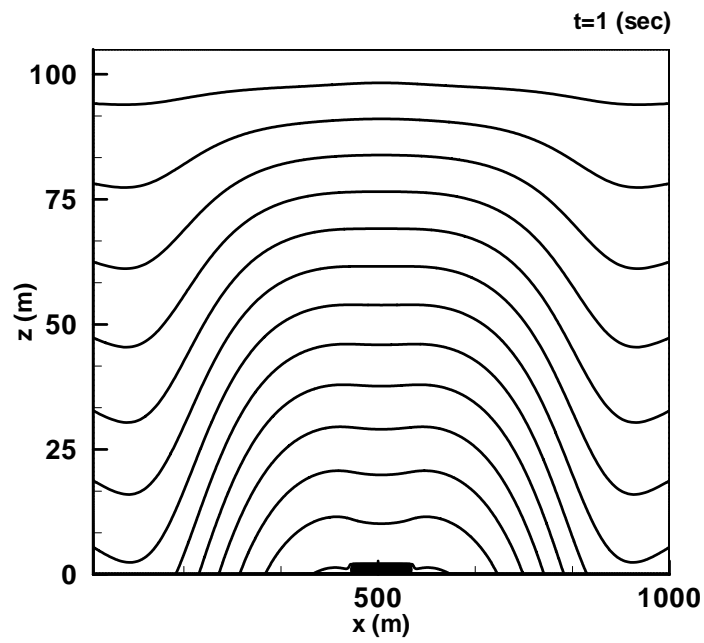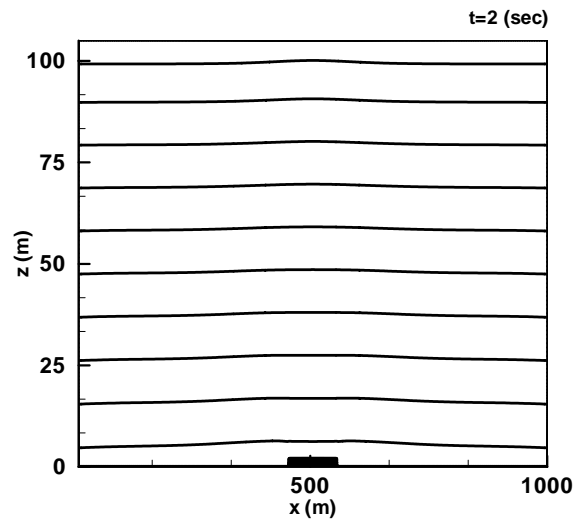
Figure 4.2 (continued)
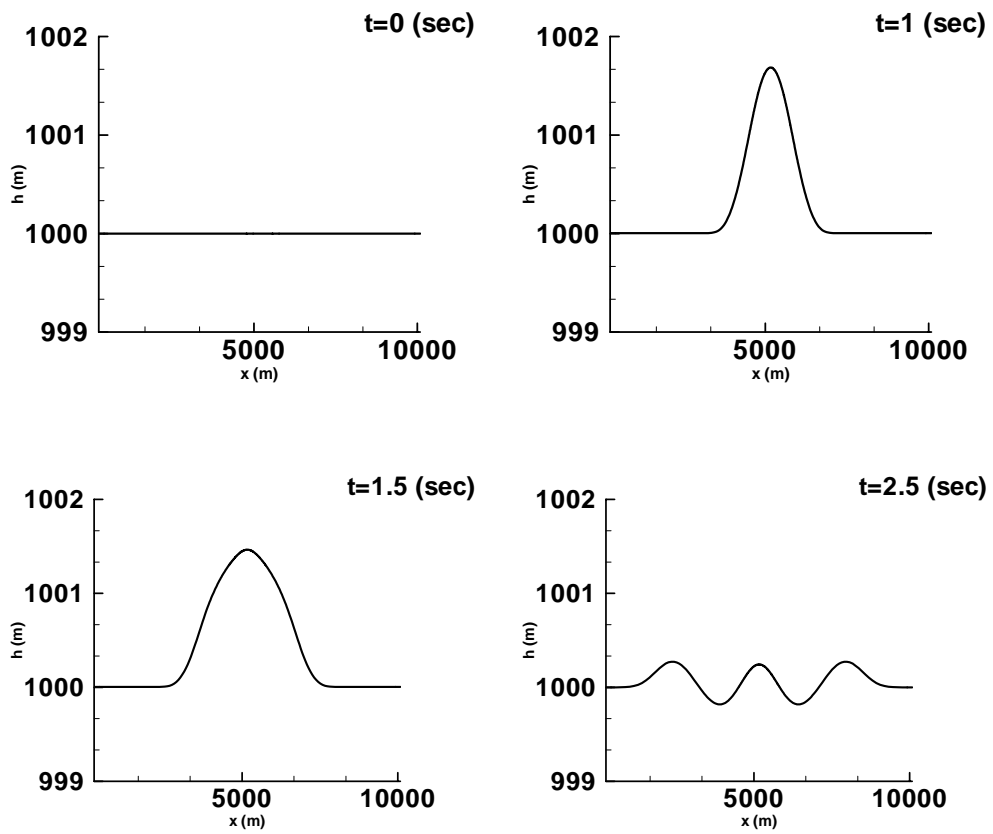
**Figure 4.3** Free surface profiles for H = 1000 m and H$_S$ = 2 m
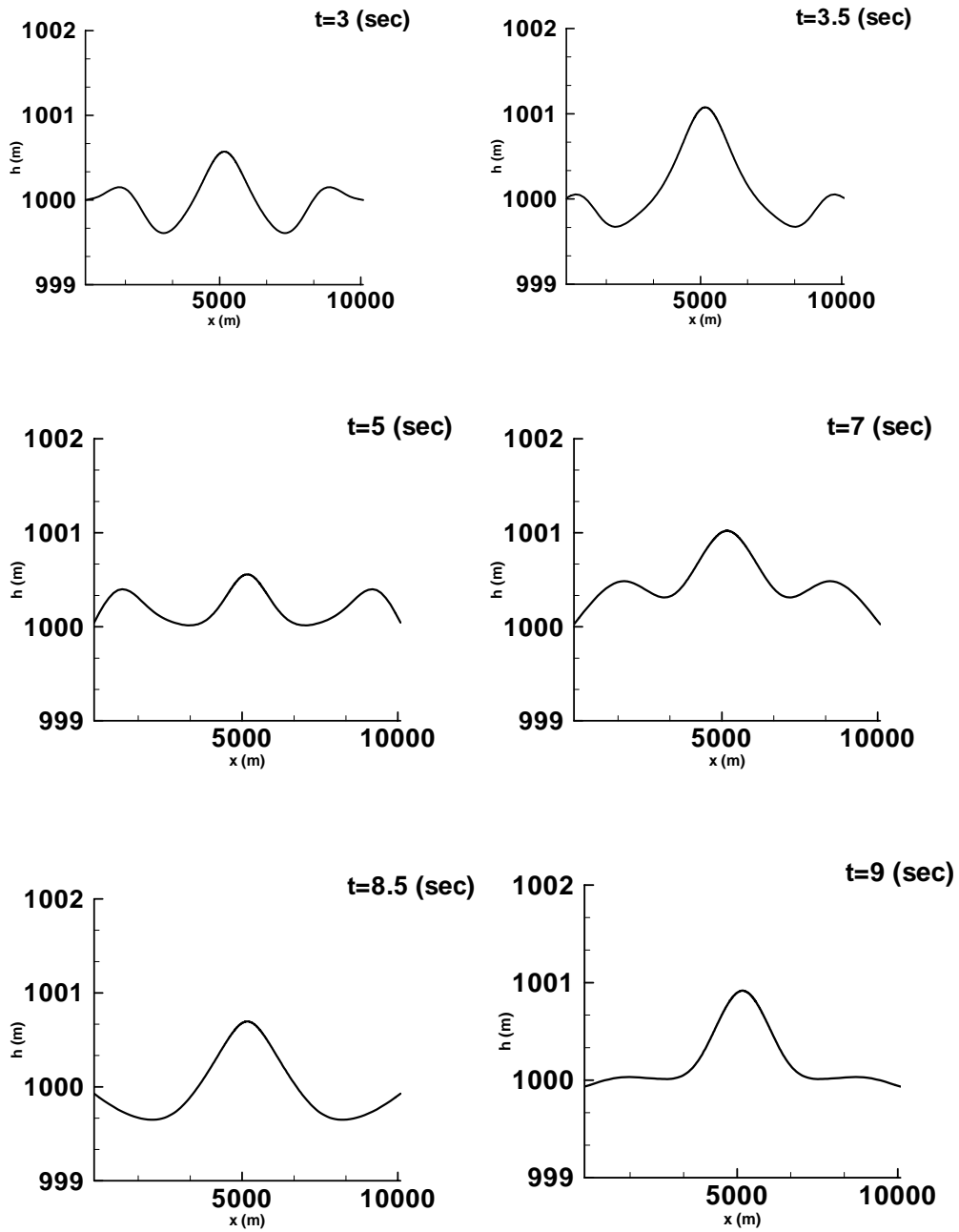
Figure 4.3 (continued)
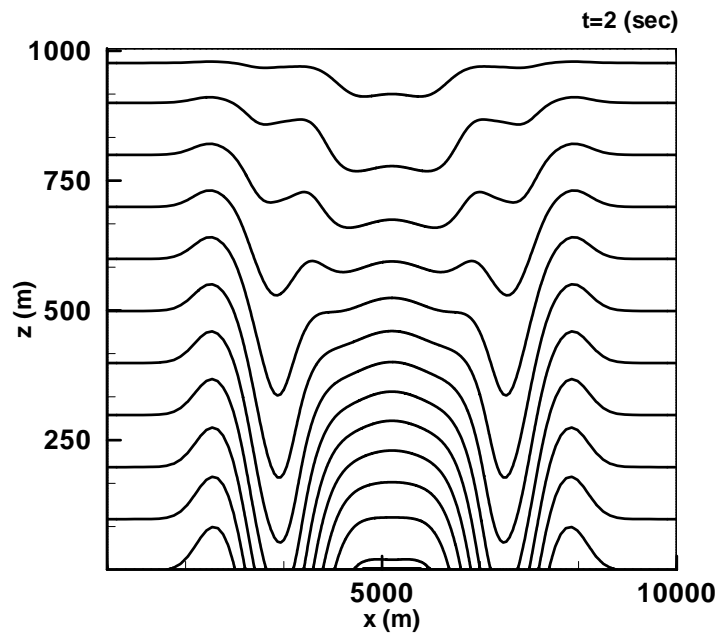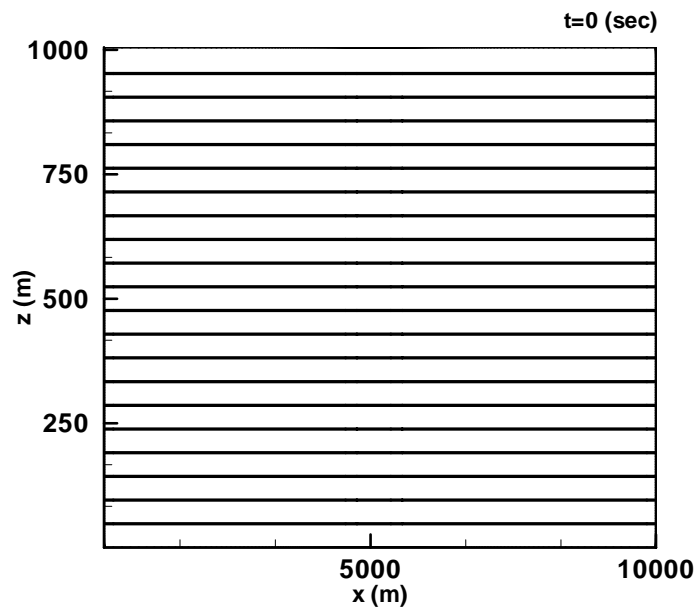
Figure 4.4 Pressure fields for H = 1000 m and H$_S$ = 2 m

**Figure 4.4 (continued)**

t=3.5 (sec)

z (m)

1000

750

500

250

5000   10000
x (m)

t=4 (sec)

z (m)

1000

750

500

250

5000   10000
x (m)

Figure 4.4 (continued)

65

t=4.5 (sec)

t=5.5 (sec)

**Figure 4.4 (continued)**

66
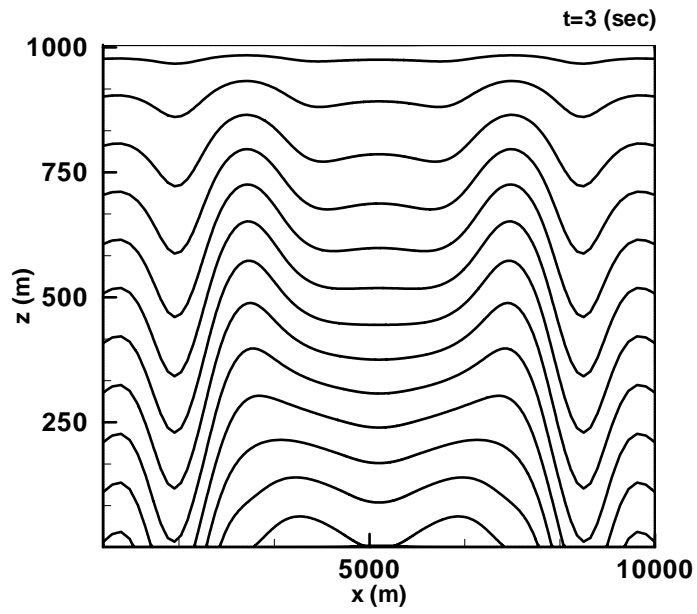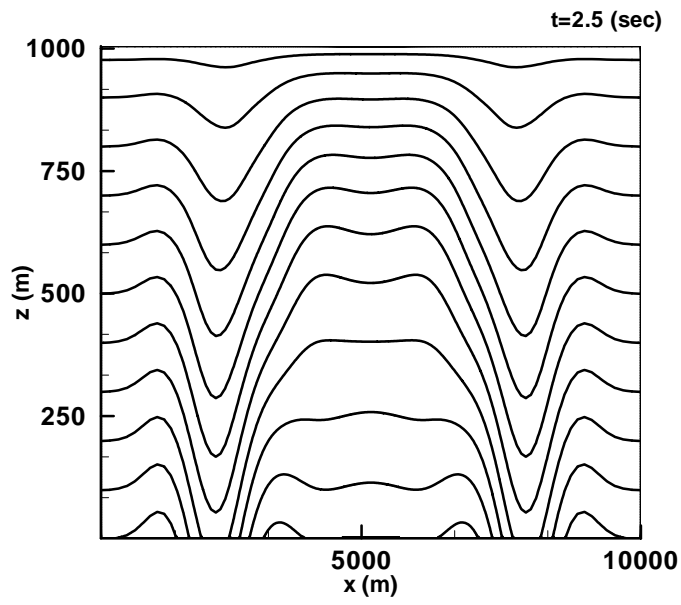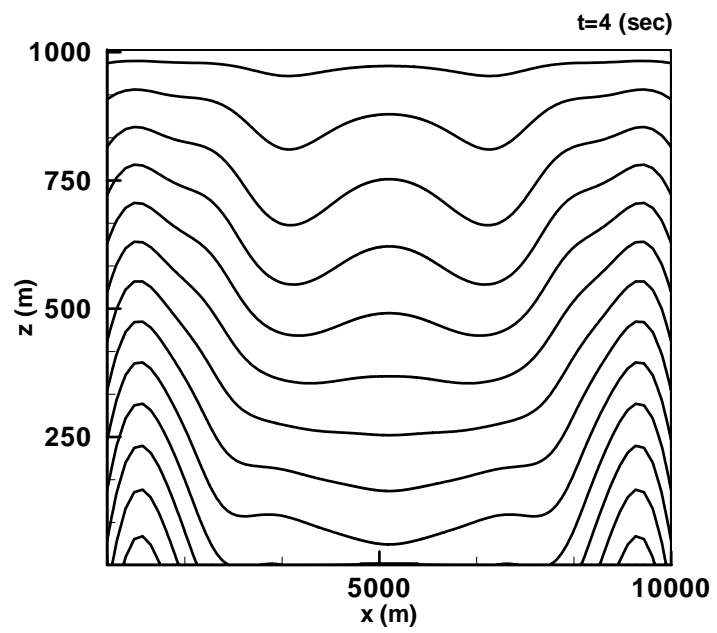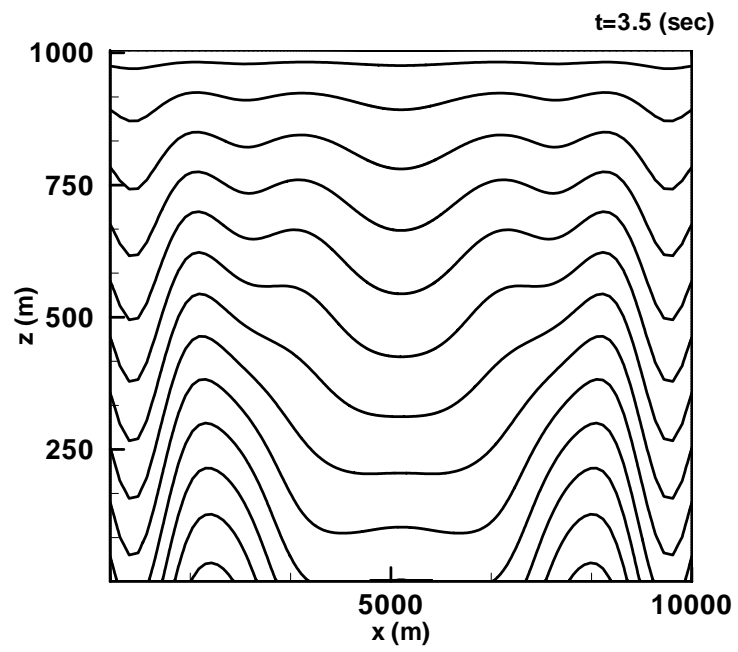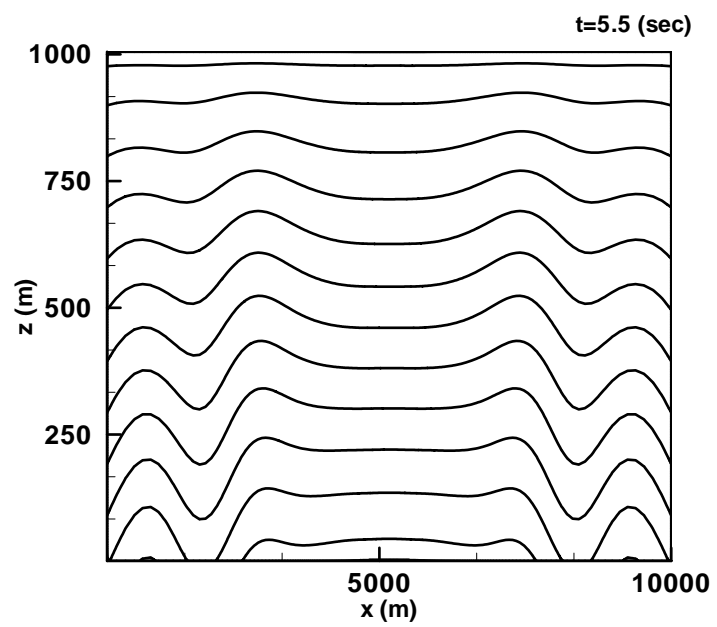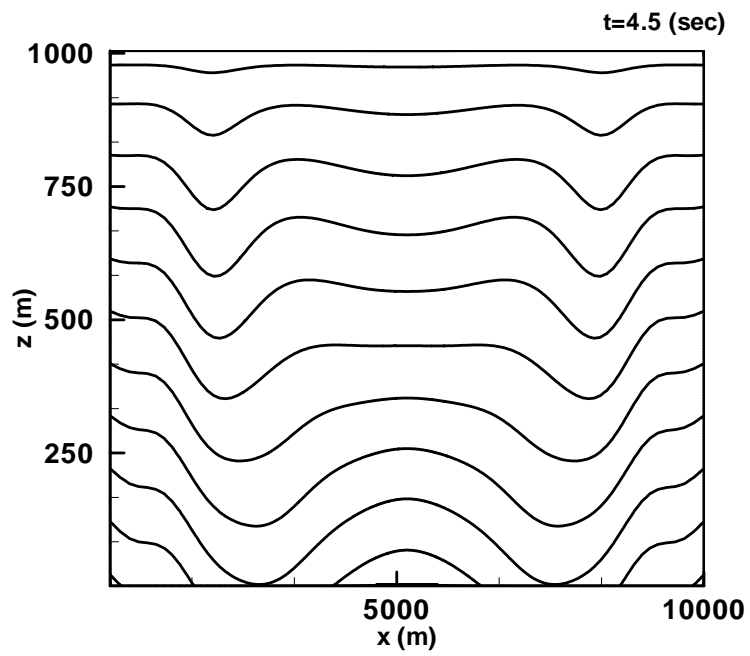
4.3 Discussions on the Results

Resulting graphs immediately divulge that the effect of the partial sea bottom motion reveals itself as a bump in the pressure contours (Figs.4.2 and 4.4) and travel to the surface. It is also observed that the velocities are distributed accordingly. As the time passes the disturbance in the pressure field dilutes away and the bump gets shorter and wider. These variations in the water bulk manifest themselves as a traveling wave on the surface. Surface waves (Figs.4.1 and 4.3) appear in the middle of the domain and travel to the sides. Since pressure distribution and the surface waves obey different equations, their time development will be different and it is readily seen in the graphs.

Similar behavior was reported previously by Kırlangıç [15]. For making a more reliable comparison, in this study, almost identical cases with H = 100 m and H = 1000 m. are tested. Pressure distributions and surface profiles as well as the maximum wave amplitudes agree quantitatively.

Besides these qualitative features, many other correlations can be investigated. The effect of compressibility can be observed more as the water gets deeper. It can be seen clearly when the pressure field plots of the case where H = 1000 m. is examined. Curvature is sharper with respect to shallower one. In addition, it takes longer time for the effect to spread out to the whole domain and dilute.

Another notable physical property is the response time of the surface to the bottom movement. For example in the case of H = 1000 m the delay is just over 3 seconds. Physical interpretation is that the pressure waves travel at the speed of sound which is about 1482 m/s in the water.

All these above results make perfect sense for the physical intuition and raise the confidence in the solution method which will be discussed in the next section.

4.4 Discussion on the Solution Method

Solution method is selected with the guidance of Kırlangıç [15] and Griebel, et. al [16]. Surface treatment completely coincides with these two works. Surface height method takes into account the fact that the real free surface can be inside the cells, so the surface cells are not totally full. All the derivatives in the calculations and boundary values are calculated accordingly as the details given in the text. Setting up a variable mesh comes in handy in this case. The minimum sizes are tried to be chosen as small as possible without making the maximum size unreasonably large.

Differences from the earlier studies should be stated here. First of all, a variable mesh in both horizontal and vertical directions is used. This enables to have greater precision in the regions where the values of computational parameters may change significantly in time such as, moving block at the bottom, the free surface and particularly in the middle areas of the domain. This goal has been reached with the same amount of computational power and memory as the study of Kırlangıç [15].

The left-right symmetry of the system is emphasized. It is enough to solve the half-domain and copy to the other side. This saves extra time and makes the algorithm much more computationally effective. With the use of symmetry property, the CPU time for a computer with 1.39 GHz, 480 MB of RAM lasts approximately 3 hours.

CHAPTER V

CONCLUSIONS

In this study, surface waves generated by sudden movements of the sea bottom are investigated in order to shed light on possible tsunami formations.

The computational domain is a two dimensional water volume on a vertical plane, where the viscosity and compressibility effects are taken into account. Marker and Cell Algorithm is used on a variable mesh in both horizontal and vertical directions.

Major conclusions of the study can be summarized as follows:

1) A rectangular grid system formed by 501x251 number of grid nodes (with appropriate clustering) is enough to obtain sufficient grid resolution.

2) Location of the far field boundary is determined from,

$$L_R = max\ (10xL_S,\ 10xH)$$

3) Surface waves are very sensitive to the velocity and accelerations of the moving block.

4) Smoothing the decelerating stage of the block in the last 25% of the period of motion is enough to eliminate the unrealistic shocks at the end of motion.

5) Block velocity must be above 4 m/s to be accounted as a rapid crack at the bottom.

6) No additional dissipation term is required in the free surface computations.

7) On the far field boundary, the first derivatives of the variable can be set to zero for an acceptable solution.

For further improvement of the model, as a recommendation, more realistic crack formations may be simulated.

REFERENCES

[1] *Wikipedia: The Free Encyclopedia.* Retrieved July 4, 2005, from
http://en.wikipedia.org/wiki/Tsunami

[2] *National Oceanic and Atmospheric Administration-The Tsunami Story.* Retrieved June 6, 2005, from http://www.tsunami.noaa.gov/tsunami_story.html

[3] *Wikipedia: The Free Encyclopedia.* Retrieved July 4, 2005, from
http://en.wikipedia.org/wiki/Tsunami#2004_-_Indian_Ocean_tsunami

[4] *The Earthquake and Tsunami of August 17, 1999 in the Sea of Marmara, Turkey-by Dr. George Pararas-Carayannis.* Retrieved May 14, 2004, from
http://www.drgeorgepc.com/Tsunami1999Turkey.html

[5] *Tsunami Laboratory, Novosibirsk, Russia.* Retrieved May 25, 2005, from
http://tsun.sscc.ru/tsulab/Med_tsu.htm#

[6] Altinok, Y., Ersoy, S., Yalciner, A. C., Alpar, B. and Kuran, U., (2001). "Historical Tsunamis in the Sea of Marmara", ITS 2001 Proceedings, Session 4, Number 4-2, 527-534.
http://www.pmel.noaa.gov/its2001/Separate_Papers/4 02_Altinok.pdf

[7] *Wikipedia: The Free Encyclopedia.* Retrieved July 8, 2005, from
http://en.wikipedia.org/wiki/Izmit_Earthquake

[8] Barka, A., Lettis, W. and Altunel, E., "Coastal Deformation Occurred During the August 17, 1999 İzmit Earthquake", Proceedings of the NATO Advanced Research Workshop on Underwater Ground Failures on Tsunami Generation, Modeling, Risk and Mitigation, Istanbul, Turkey, May 23–26, 2001.

[9] Lynett, P. and Liu, P. L. F "Submarine Landslide Generated Waves Modeled Using Depth-Integrated Equations", Proceedings of the NATO Advanced Research Workshop on Underwater Ground Failures on Tsunami Generation, Modeling, Risk and Mitigation, Istanbul, Turkey, May 23–26, 2001.

[10] Todorovska, M. I., Hayir, A. and Trifunac, M. D., "Near Field Amplitudes of Tsunami from Submarine Slumps and Slides", Proceedings of the NATO Advanced Research Workshop on Underwater Ground Failures on Tsunami Generation, Modeling, Risk and Mitigation, Istanbul, Turkey, May 23–26, 2001.

[11] Fine, I. V., Rabinovich, A. B., Thomson, R. E. and Kulikov, E. A., "Numerical Modeling of Tsunami Generation by Submarine and Subaerial landslides", Proceedings of the NATO Advanced Research Workshop on Underwater Ground Failures on Tsunami Generation, Modeling, Risk and Mitigation, Istanbul, Turkey, May 23–26, 2001.

[12] Ohmachi, T., "Tsunami Simulation Taking Into Account Seismically Induced Dynamic Seabed Displacement and Acoustic Effects of Water", Proceedings of the NATO Advanced Research Workshop on Underwater Ground Failures on Tsunami Generation, Modeling, Risk and Mitigation, Istanbul, Turkey, May 23–26, 2001.

[13] Tyvand, P. A., Miloh, T. and Haugen, K. B., "Impulsive Tsunami Generation by Rapid Bottom Deflections at Initially Uniform Depth", Proceedings of the NATO Advanced Research Workshop on Underwater Ground Failures on Tsunami Generation, Modeling, Risk and Mitigation, Istanbul, Turkey, May 23–26, 2001.

[14] Matsuyama, M. and Yeh, H., "Effects of Tsunami at Sissano Lagoon, Papua New Guinea: Submarine-Landslide and Tectonics Origins", Proceedings of the NATO Advanced Research Workshop on Underwater Ground Failures on Tsunami Generation, Modeling, Risk and Mitigation, Istanbul, Turkey, May 23–26, 2001.

[15] Kırlangıç, Ö., (2004)."Generation of Surface Waves due to Sudden Movements at the Sea Bottom", M.Sc. Thesis, Metu.

[16] Griebel, M., Dornseifer, T. and Neunhoeffer, T., (1998). "Numerical Simulation in Fluid Dynamics : A Practical Introduction", Society for Industrial and Applied Mathematics, Philadelphia.

[17] Nosov, M. A. and Kolesov, S. V., "Tsunami Generation in Compressible Ocean of Variable Depth", Proceedings of the NATO Advanced Research Workshop on Underwater Ground Failures on Tsunami Generation, Modeling, Risk and Mitigation, Istanbul, Turkey, May 23–26, 2001.

[18] *Density of Ocean Water.* Retrieved August 31, 2001, from
http://www.windows.ucar.edu/tour/link=/earth/Water/density.html&edu=high

[19] *Physical Properties of Sea Water.* Retrieved June 10, 2000, from
http://sam.ucsd.edu/sio210/proseawater/ppsw_fortran/rho.f

[20] Arkhipkin, V. S. & S. A. Dobrolubov, 1999. Steric variation of the Mediterranean and Black Sea level. In E. Th. Balopoulos & A. Iona (eds), Oceanography of the Eastern Mediterranean and Black Sea, Sakellariou, Athens: 5 6.

[21] Hirt, C. W. and Nichols, B. D., (1980). "Adding Limited Compressibility to Incompressible Hydrocodes", J. Comput. Phys., 34, 390-400.

[22] Nichols, B. D. and Hirt C. W., (1973). "Calculating Three-Dimensional Free Surface Flows in the Vicinity of Submerged and Exposed Structures", J. Comput. Phys., 12, 234-246.

[23] Hirt, C. W. and Nichols, B. D., (1981). "Volume of Fluid (VOF) Method for the Dynamics of Free Boundaries", J. Comput. Phys., 39, 201-225.

[24] Nichols, B. D. and Hirt C. W., (1971). "Improved Free Surface Boundary Conditions for Numerical Incompressible-Flow Calculations", J. Comput. Phys., 8, 434-448.